Nanomaterials

for high tech applications

Nano Tech 2011

Tokyo, 16 – 18 February

Silver nanowire networks as flexible, transparent, conducting films

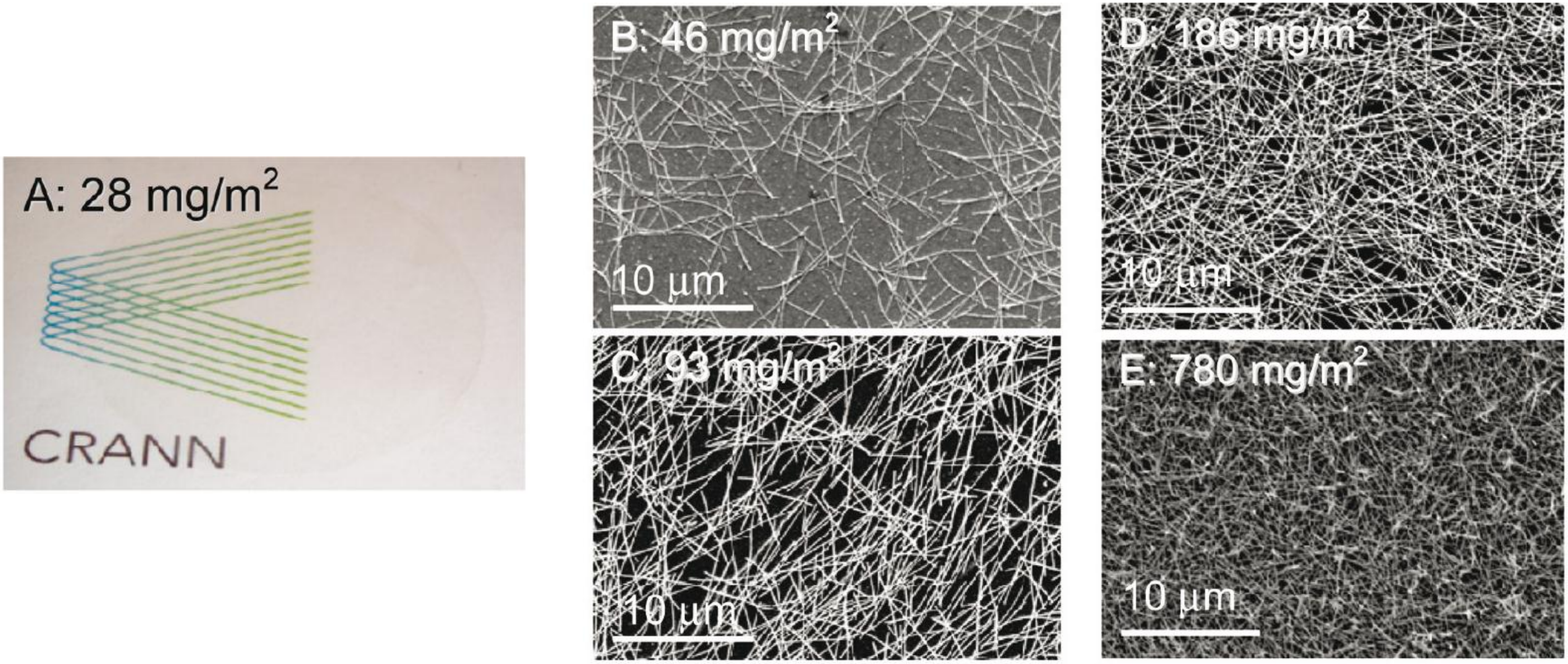

(A) Photograph of a film of AgNWs on PET covering the CRANN logo. (B - E) SEM images of the surfaces of films of increasing thickness, 46 < M/A < 780 mg/m^2.

Palladium nanowires for hydrogen sensors

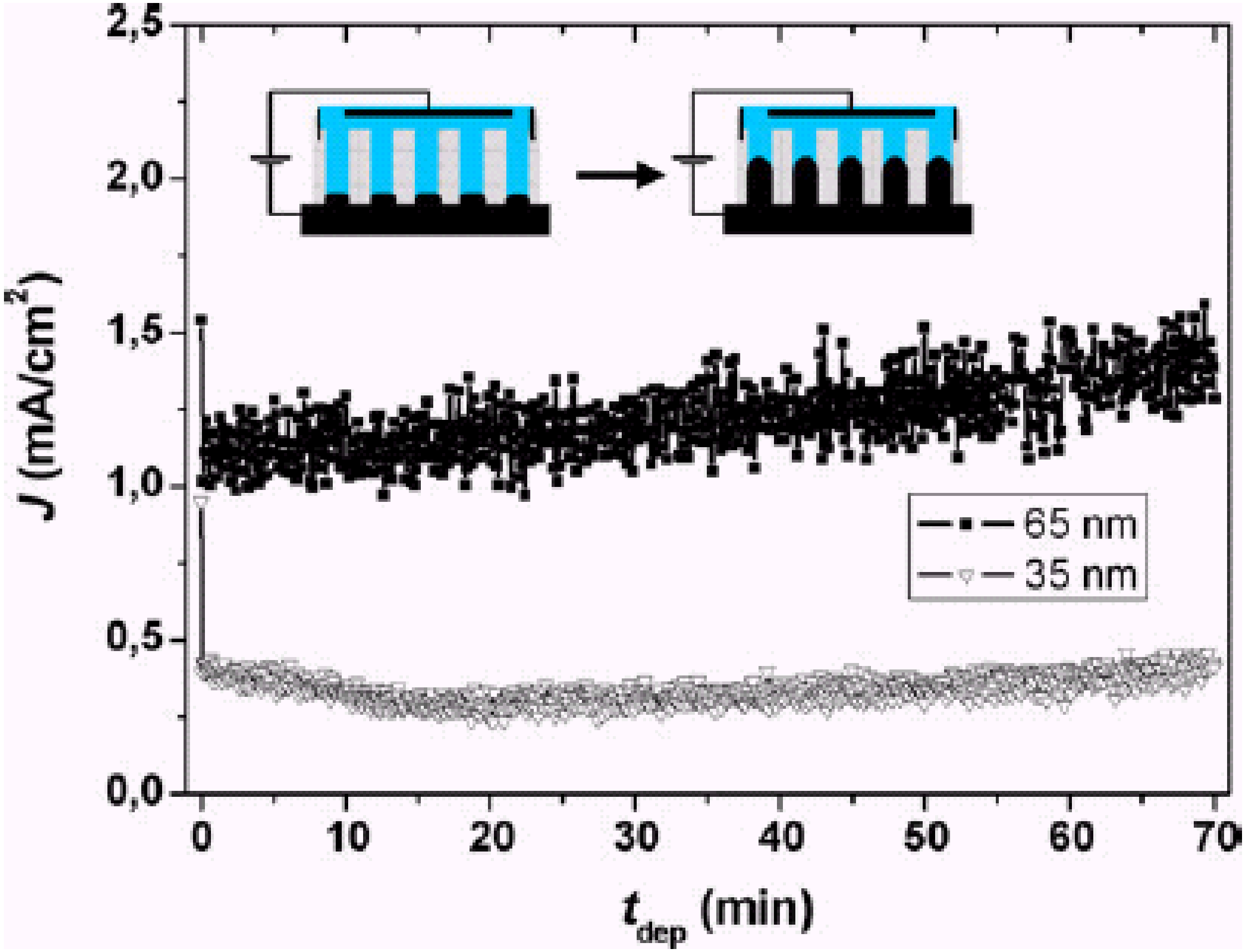

Palladium membrane for hydrogen separators

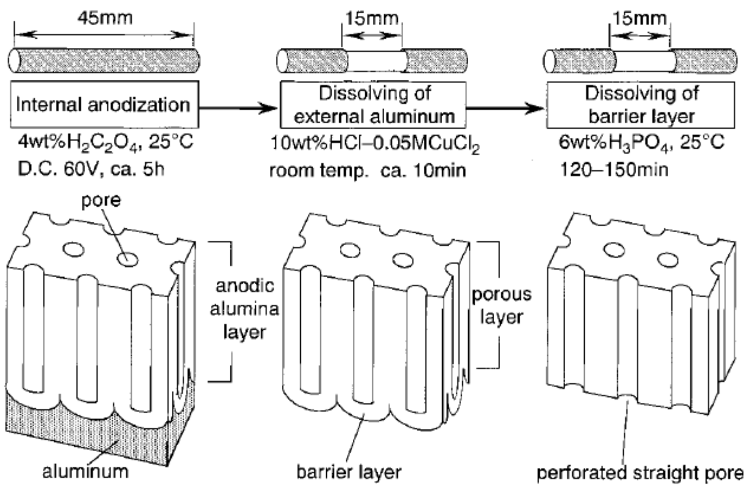

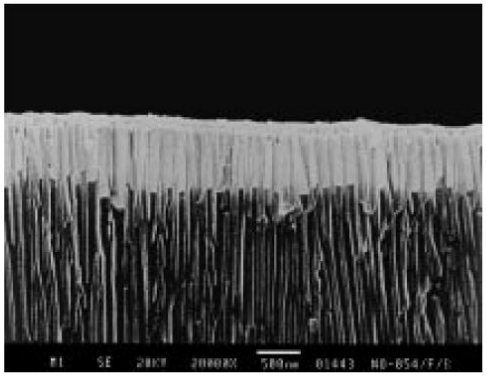

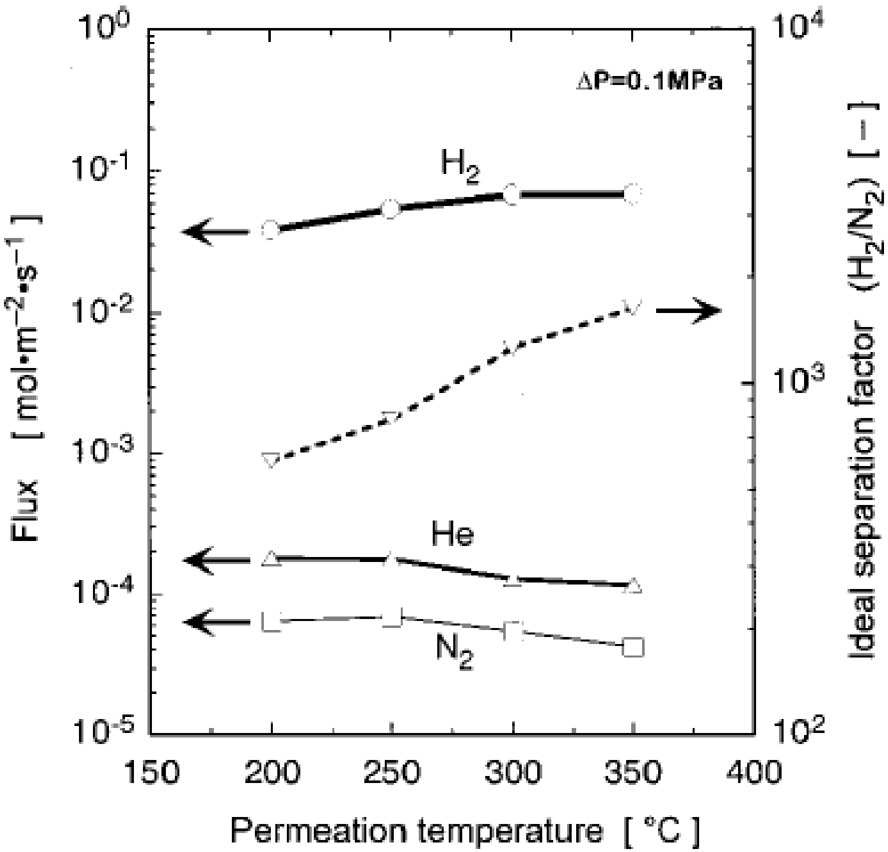

N. Itoh et al. / Microporous and Mesoporous Materials 39 (2000) 103±111

Porous alumina templates and nanostructured CdS for thin film solar cell applications

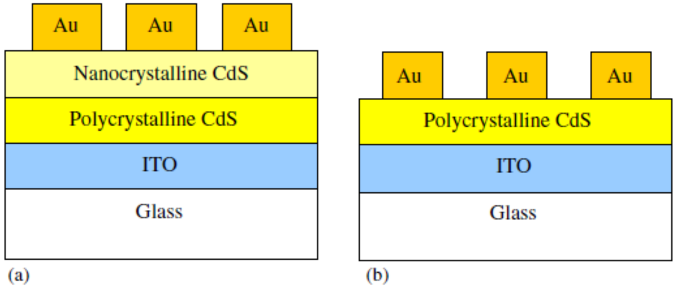

Current–voltage characteristics of polycrystalline CdS/Au and polycrystalline CdS/nanocrystalline CdS/Au devices.

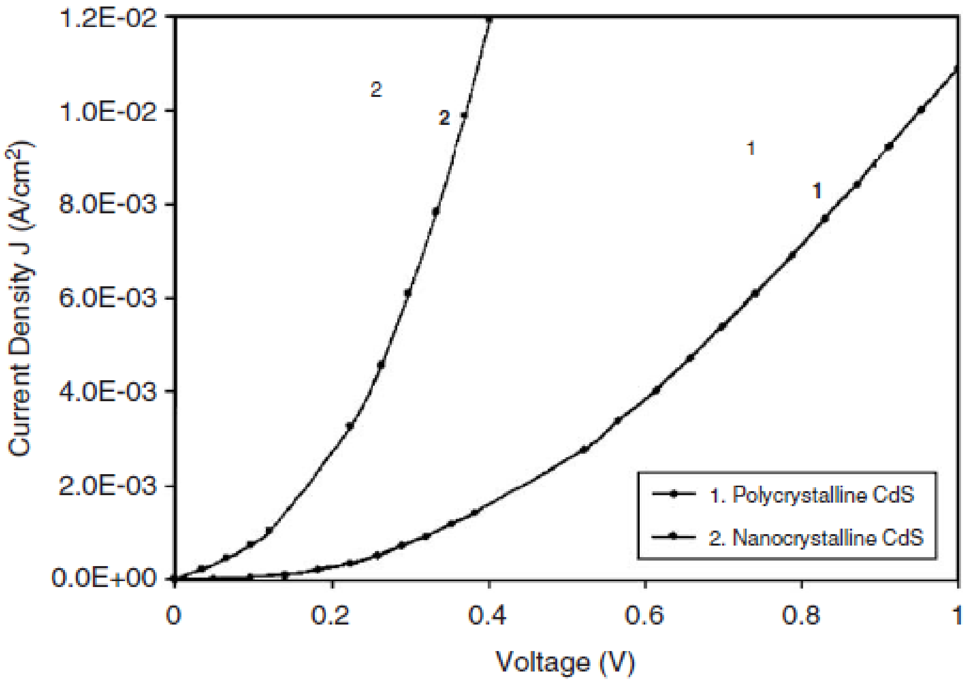

High-efficiency solar cells based on semiconductor nanostructures

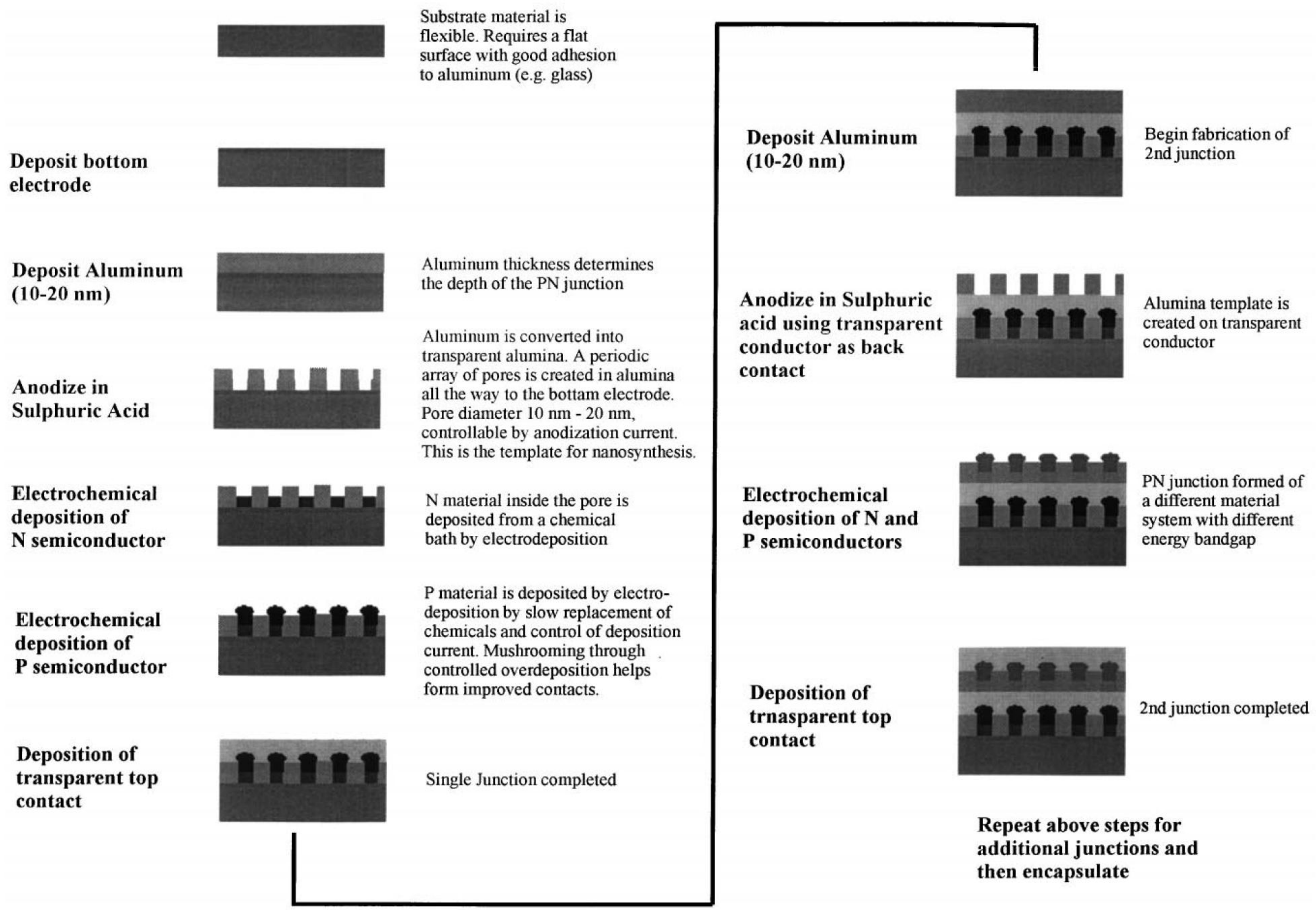

Position particle detector

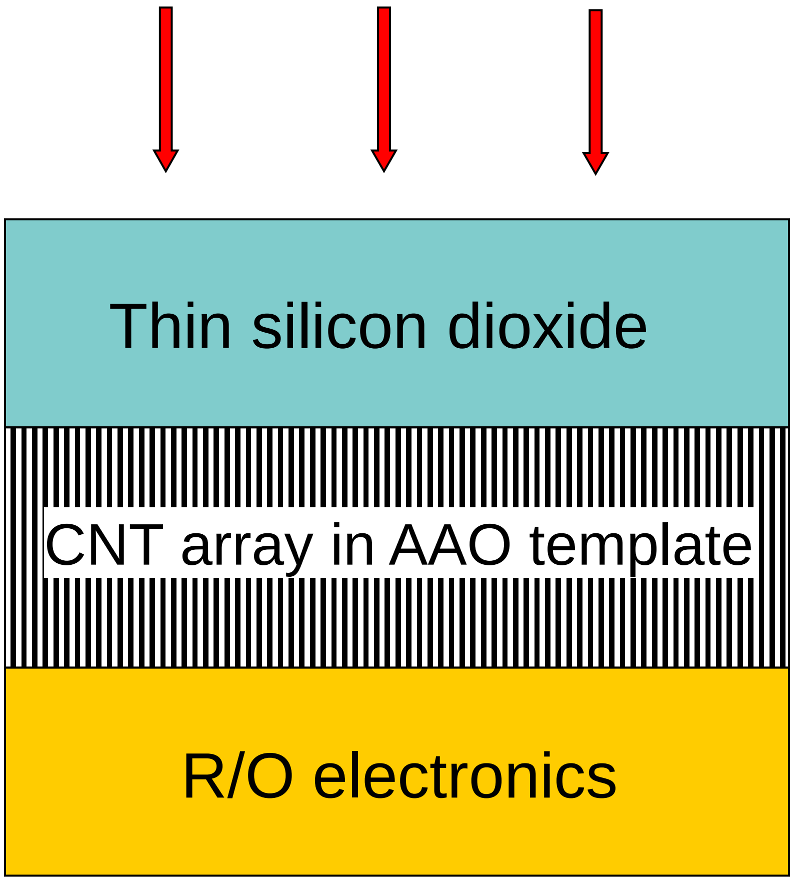

A regular and uniform matrix of carbon nanotubes, grown inside the alumina template, is sandwiched between an active layer and a readout layer.

The active layer is formed formed by a reverse biased silicon diode, in which a charged particle produces electro-hole pairs during its passage.

The readout layer is constituted by CMOS electronics embedded in a silicon substrate.

R.Angelucci et al.,/ Nuclear Physics B (Proc. Suppl.) 125 (2003) 164-168

Gas ionization sensors

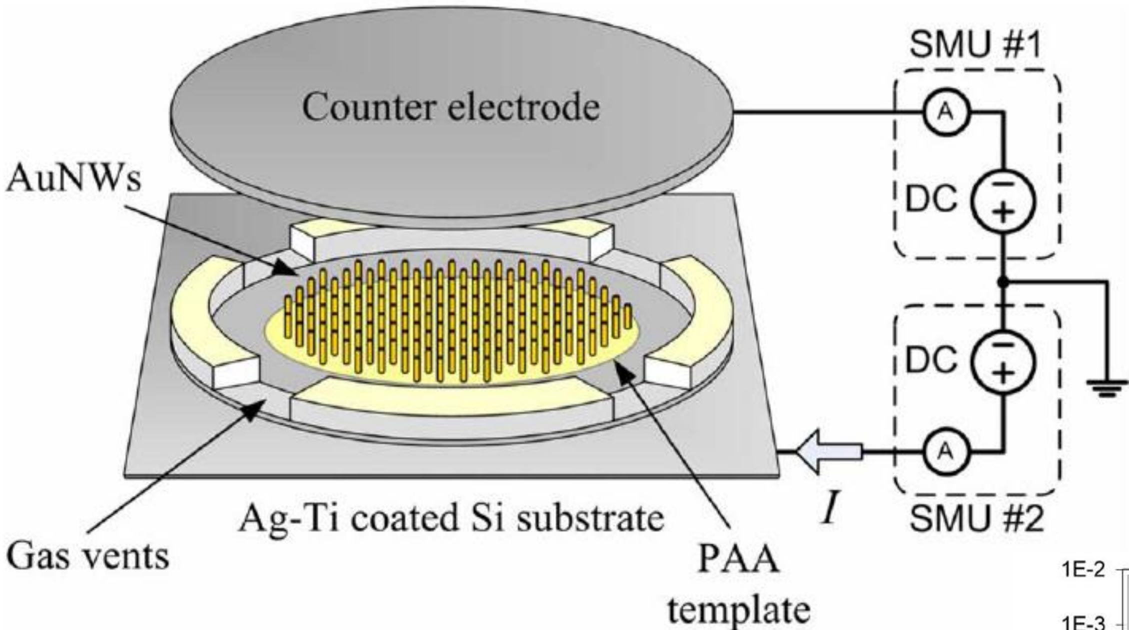

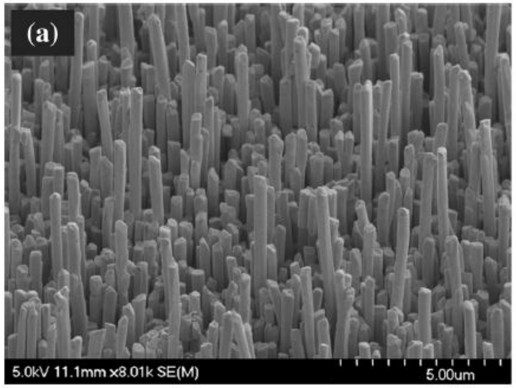

Room temperature FI I –V curves of helium in different pressures (P = 0:01, 0.1, 1, 10, and 100 torr)

Four different regimes:1) ohmic (pre-ionization); 2) field-limited; 3) intermediate; and 4) supply-limited.

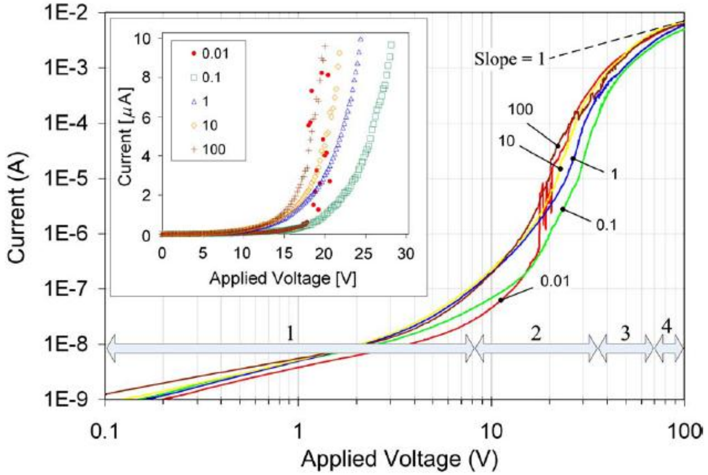

Ammonia and humidity sensor

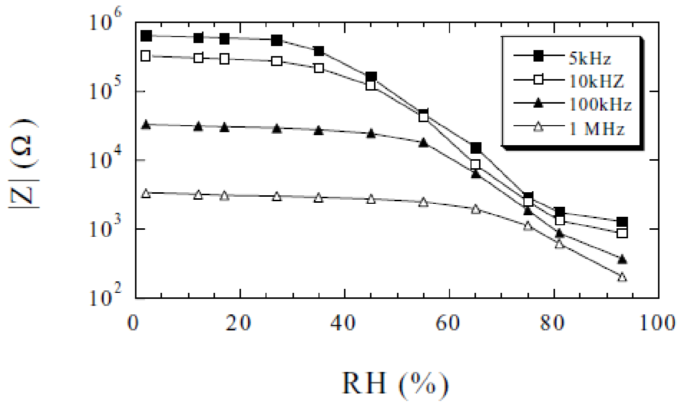

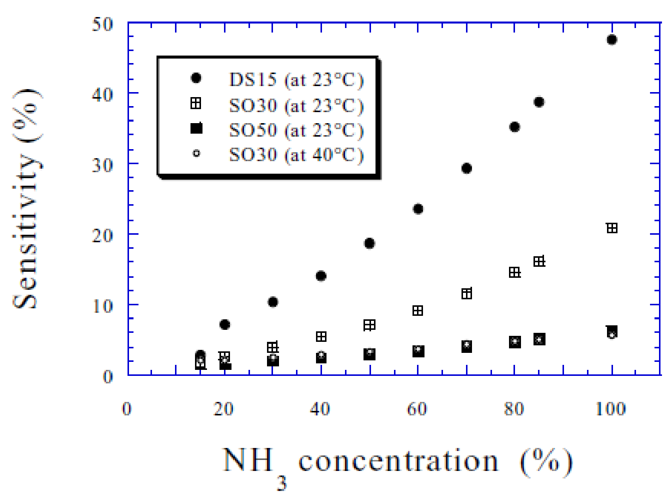

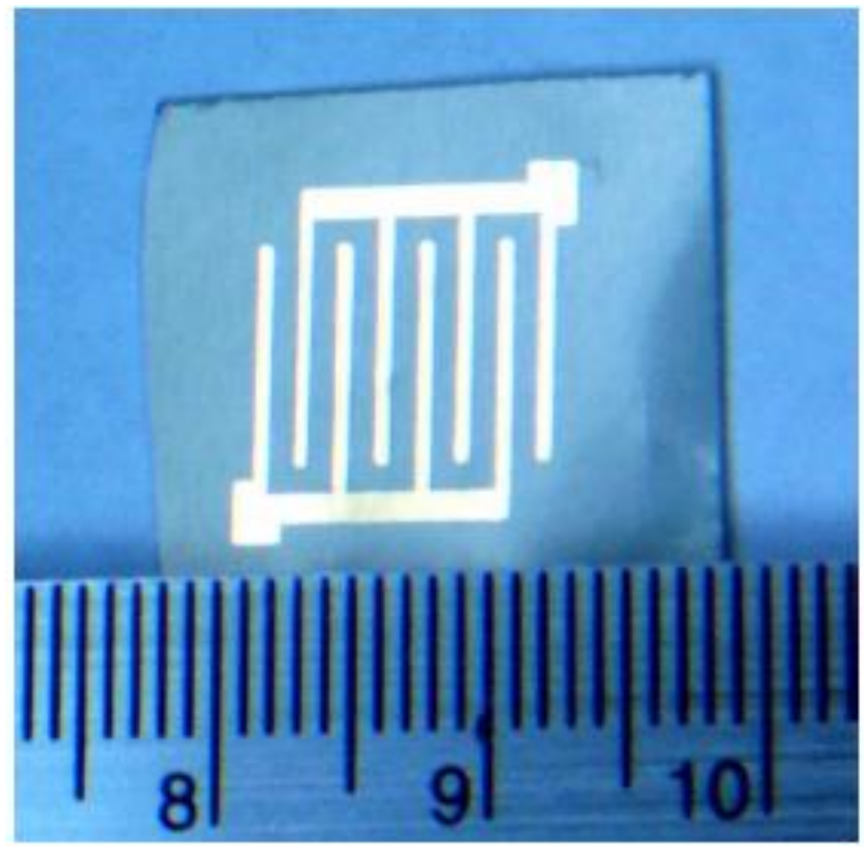

E. C. Dickey/ *et al. Sensors* ***2002, 2, 91-110***

Transfer of the AAO pattern into a Si substrate

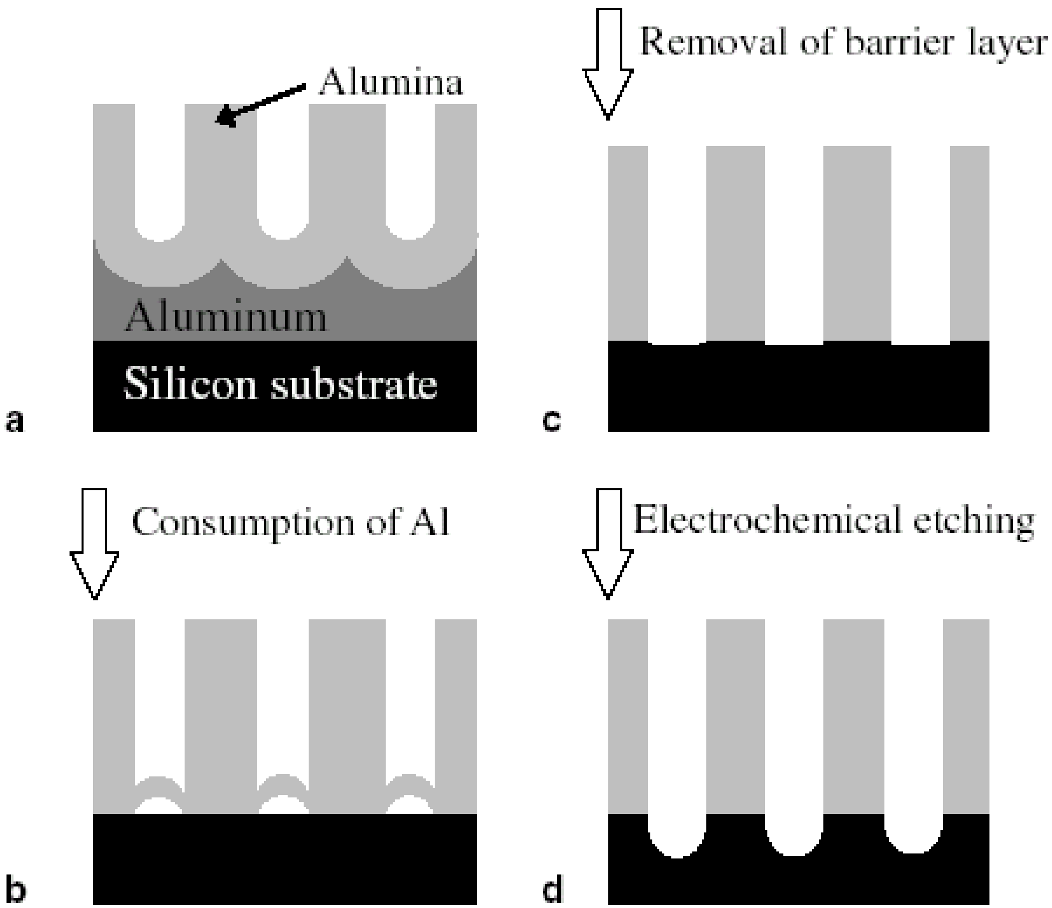

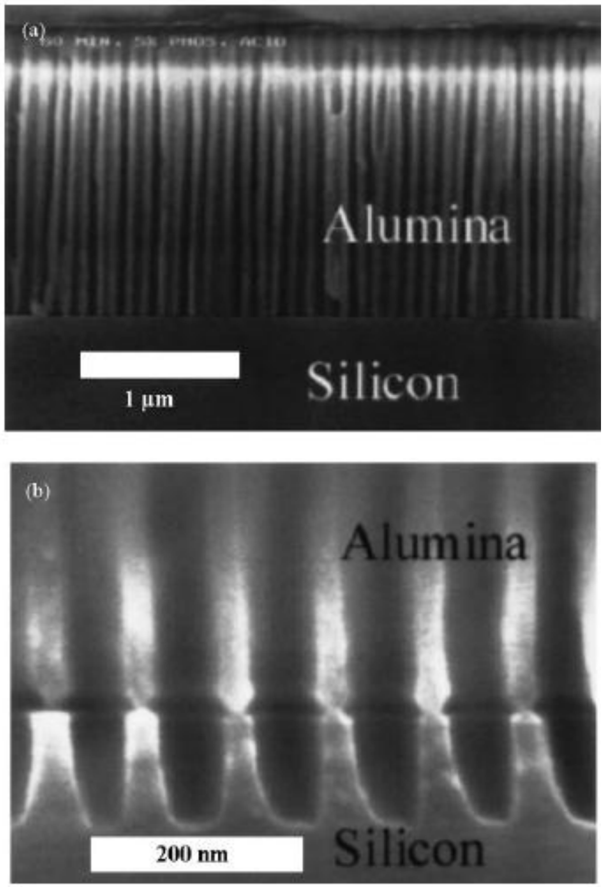

H. Asoh,/ Electrochem Comm 7 (2005) 953–956.; H. Chik, J.M. Xu / Materials Science and Engineering R 43 (2004) 103–138

Nanostructures on glass by

Al anodization and electrodeposition

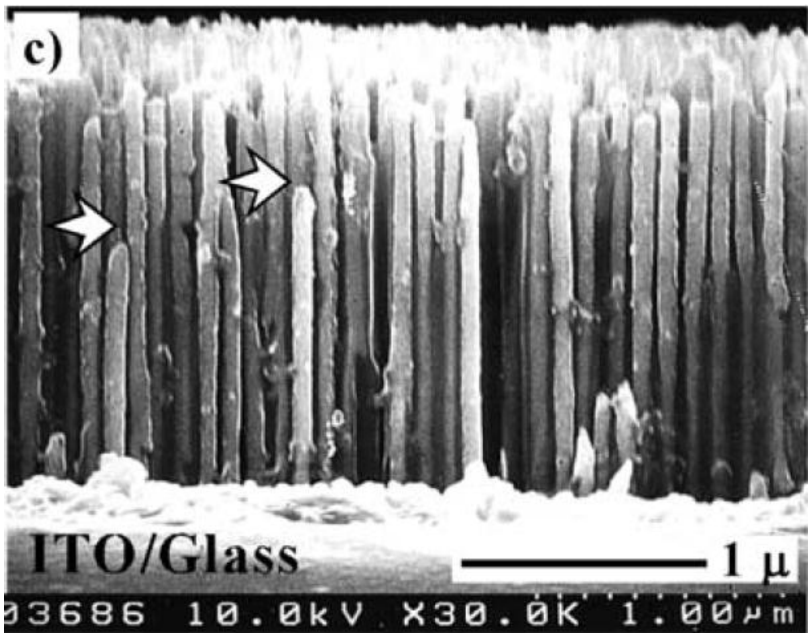

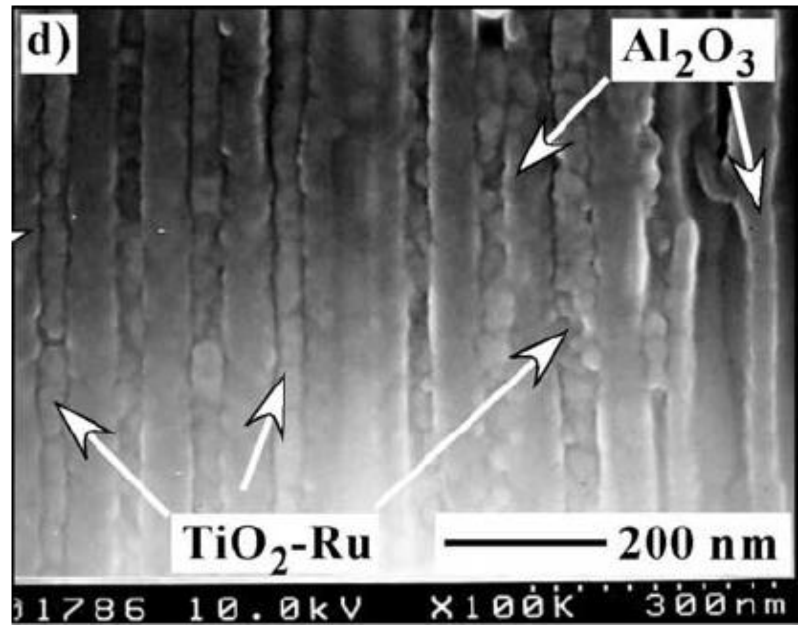

Nickel nanowire arrays in porous alumina films on the ITO/glass substrate.

TiO_2/RuO_2 in the porous alumina films on ITO/glass.

S.Z. Chu et el. / Electrochimica Acta 48 (2003) 3147-3153.

A μ-sized nanoporous multifunction capacitive sensing device

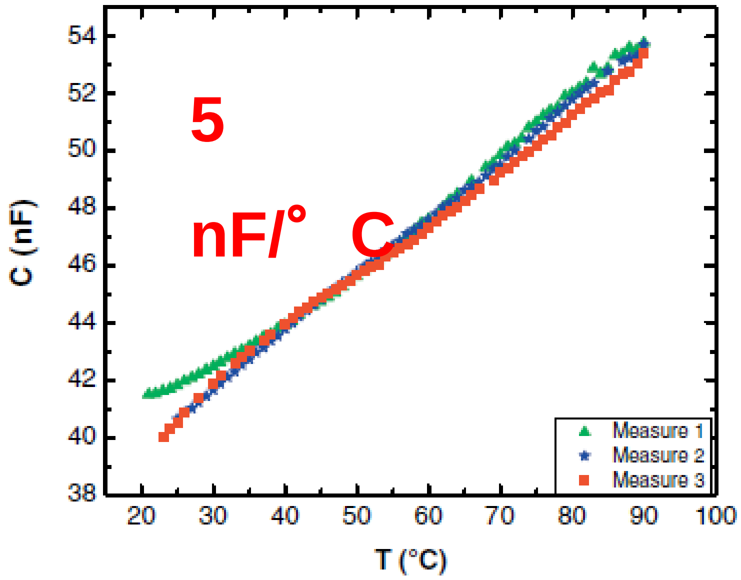

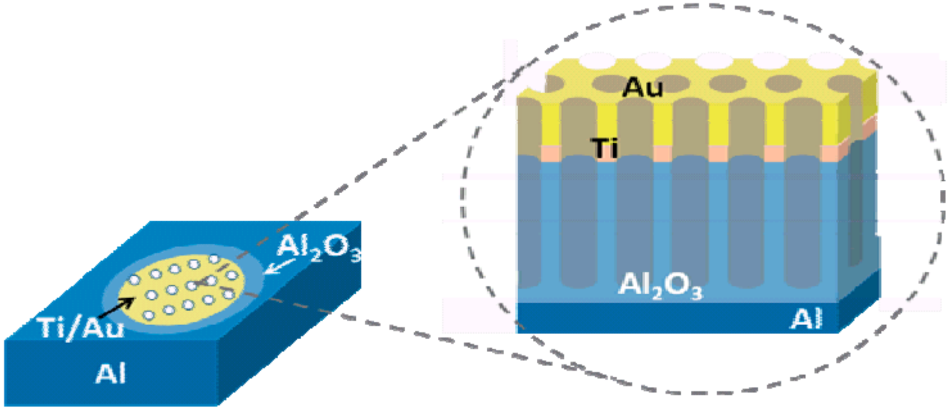

Detection of DNA oligonucleotides on nanowire array electrodes using chronocoulometry

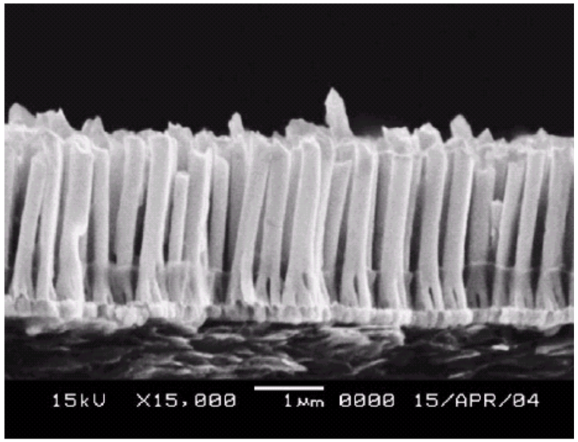

Nanowire array electrode

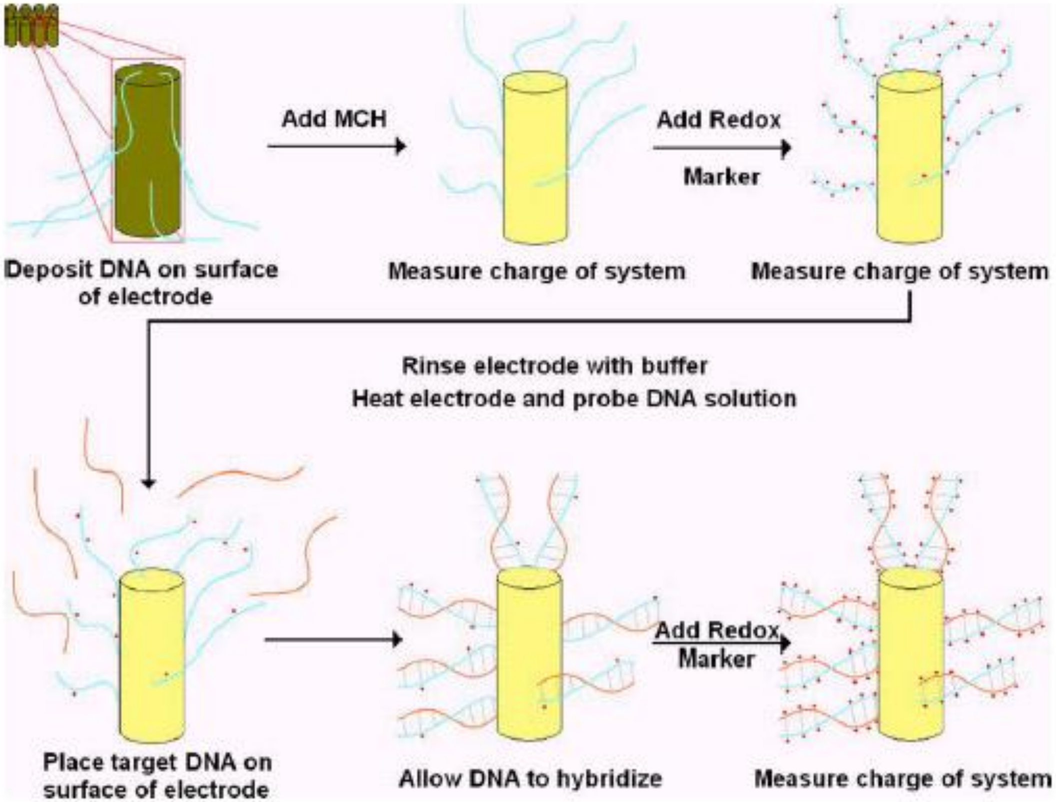

Nanoelectrode arrays for glucose biosensors

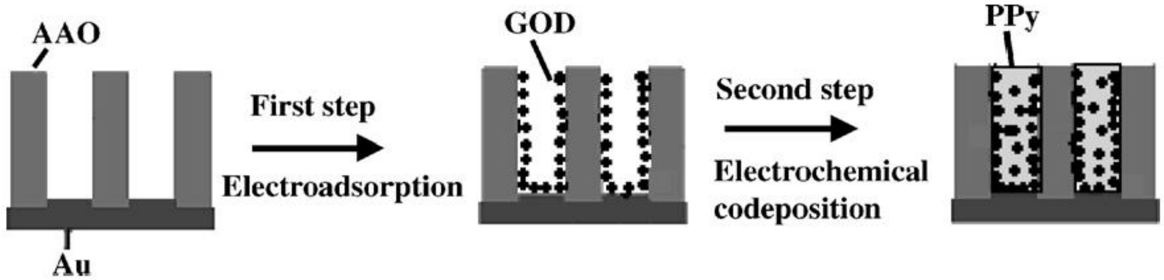

Preparation process of Au-AAO/GO_X/PPy nanofiber array electrode.

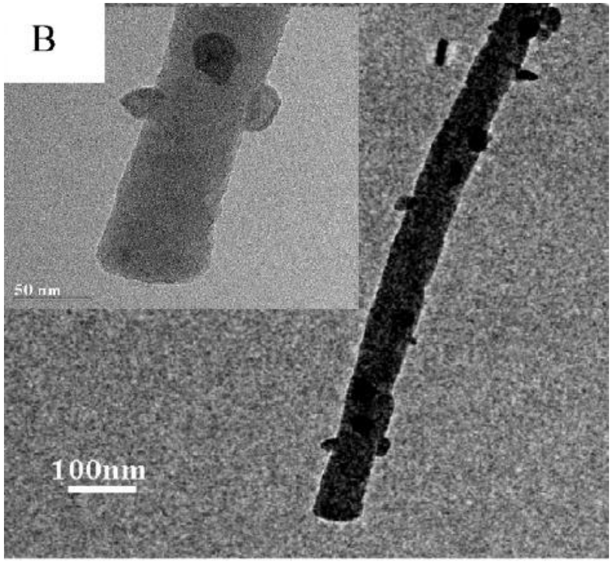

TEM image of PPy/GO_X nanofiber

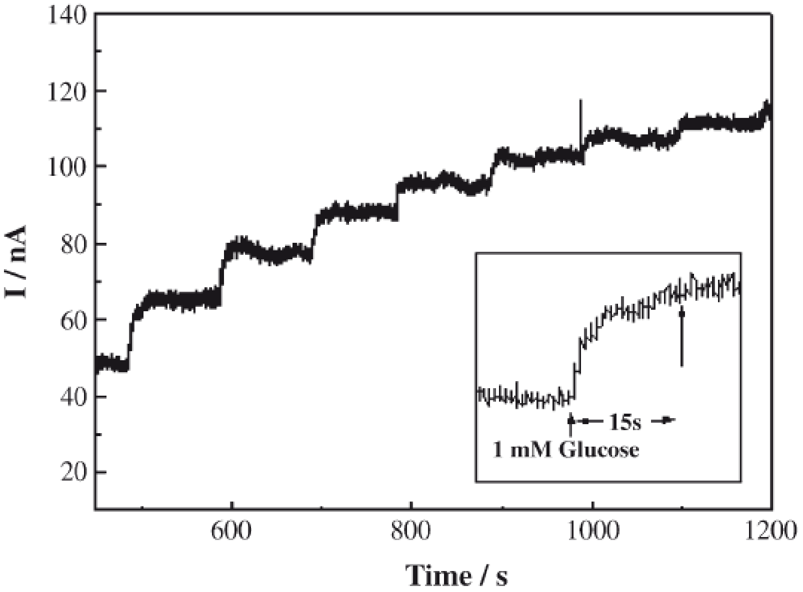

Amperometric response of Au-AAO/GO_X/PPy array electrode to the glucose addition (pH 6.86; E 0.6 V)

L. Liu et al. / Materials Science and Engineering C 27 (2007) 57–60

Oxidation of glusose to gluconolactone

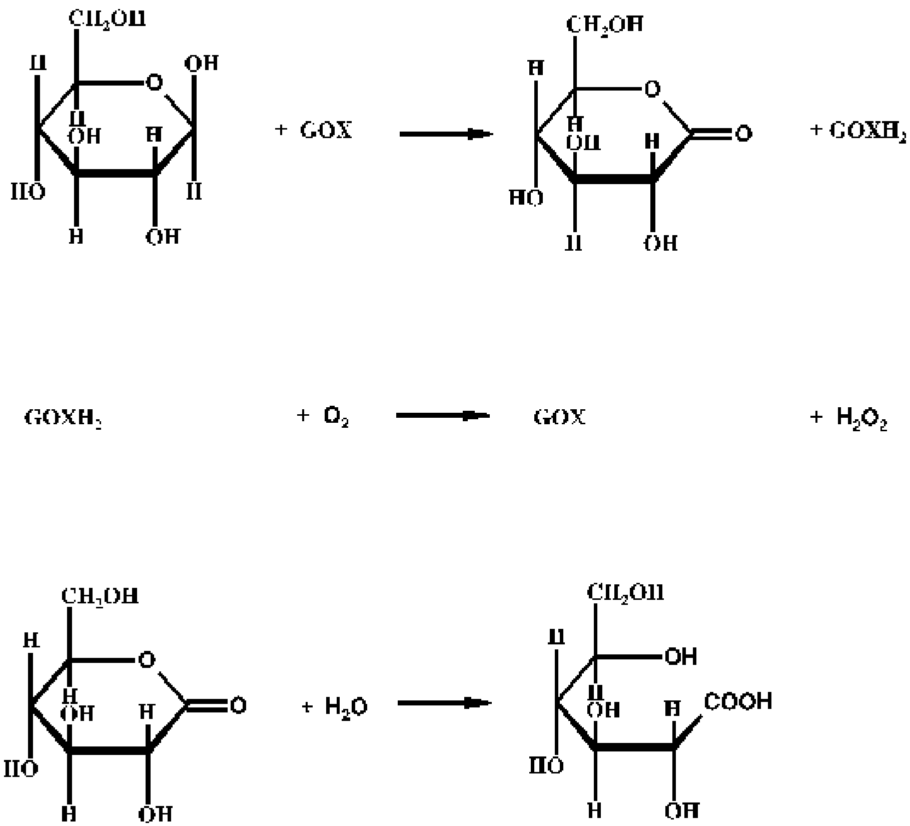

The GOX-based glucose biosensors catalyzes the oxidation f glucose to gluconolactone in the presence of oxygen, producing H_2O_2. Quantification of glucose is achieved via electrochemical oxidation of the liberated H_2O_2 ($H_2O_2 \rightarrow O_2 + 2H^+ + 2e^-$).

Nanoelectrode arrays for glucose biosensors

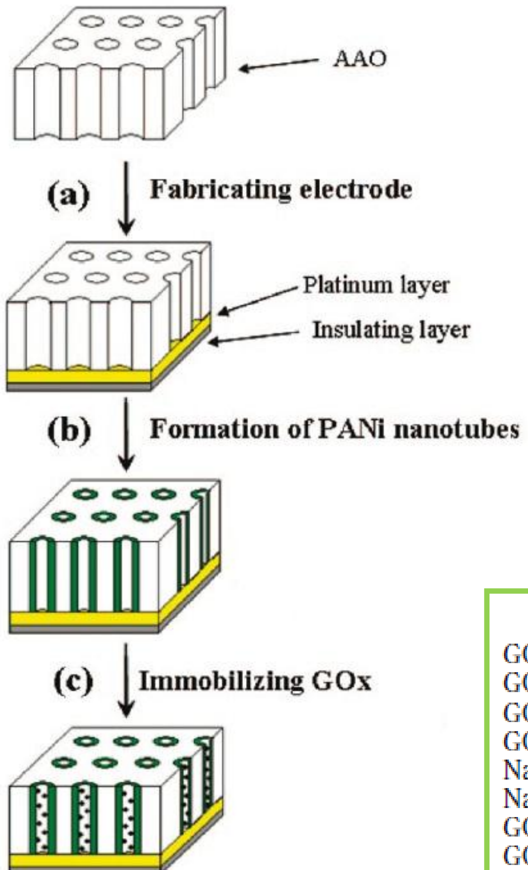

Preparation process of GO_X-nanoPANi array electrode

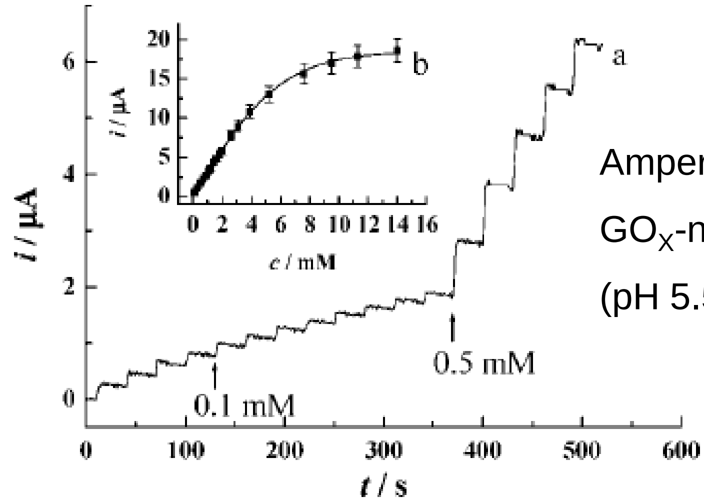

Amperometric response of GO_X-nanoPANi array electrode (pH 5.5; E -0.3 V SCE)

Comparison of analytical performance of some glucose biosensors

glucose biosensor	sensitivity (μA mM^{-1} cm^{-2})	detection limit (μM)	response time (s)
GOx-nanoPANi	97.18 ± 4.62	0.3 ± 0.1	~3
GOx-sol−gel-chitosan	0.274	10	<30
GOx-sol−gel-CNTs[a]	0.2	50	5
GOx-polypyrrole	0.007		15
Nafion-GOx-OMC[b]	0.053	156.52	9 ± 1
Nafion-GOx-SWCNH[c]	1.06	6	
GOx-Nb-SWNT[d]		10	5
GOx-PANAA[e]	6.82	0.5	<30
GOx-polyacrylonitrile	4.2	20	~20
GOx-poly(*o*-aminophenol)		0.5	4
GOx-TEOS-sol−gel[f]		200	30
GOx-PPy/*o*PPD[g]	0.019	5.14	5.1
GOx-redox polymer[h]			10

Z. Wang et al. / Anal.Chem. 81 (2009) 1638-1645

Label-free optical biosensors

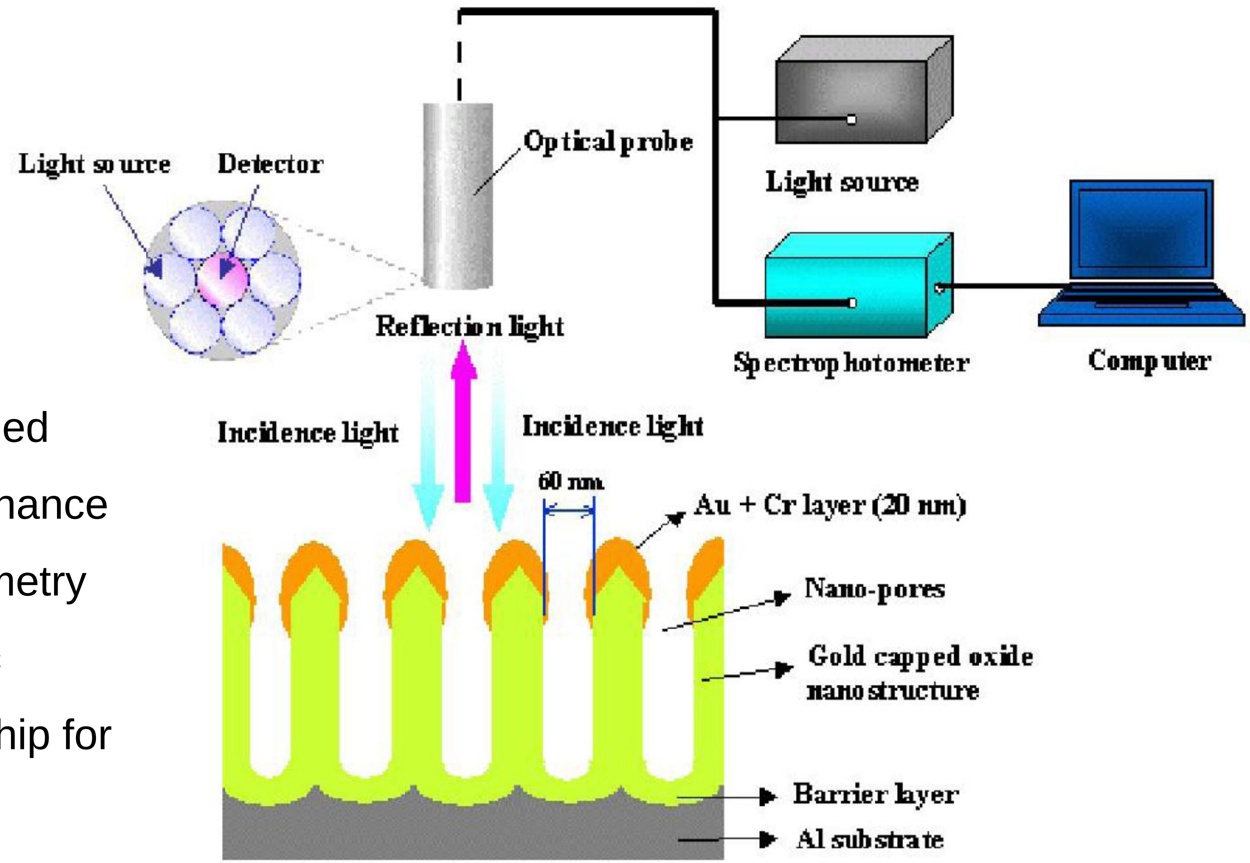

Combination of localized surface plasmon resonance (LSPR) with interferometry using a porous anodic alumina layer (PAA) chip for the detection of DNA hybridization

Label-free DNA sensor based on surface charge modulated ionic conductance

Gold electrodes deposited directly on its opposite sides and the surface of nanopores modified by an mixture of neutral ester silanes and morpholinos (neutral analogue of DNA).

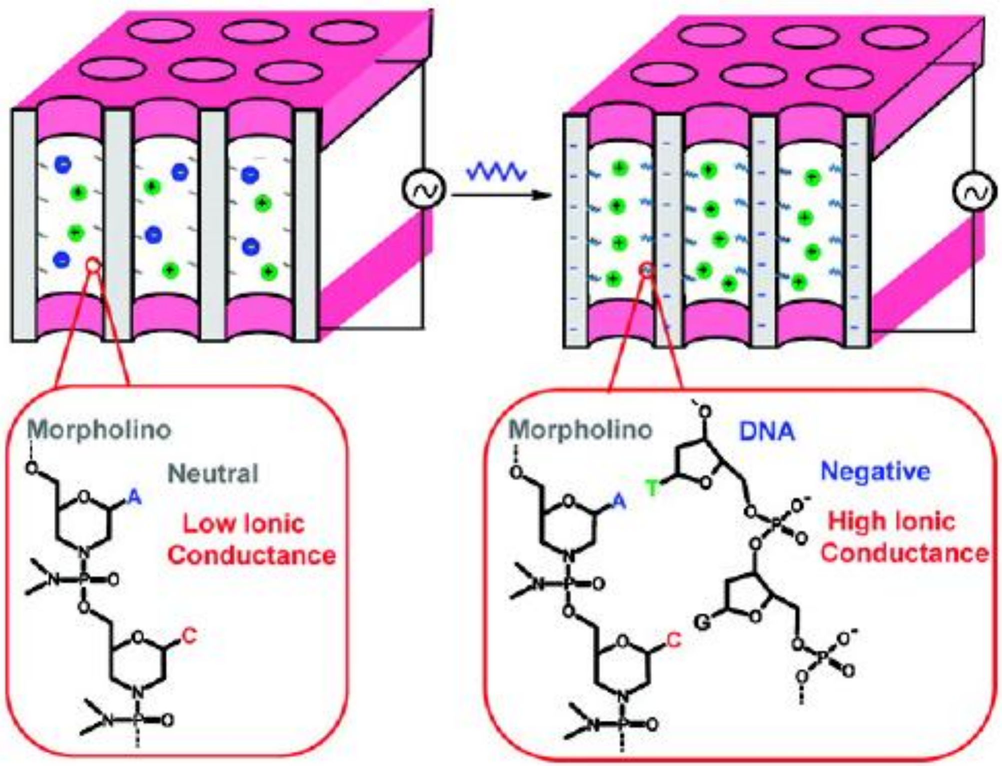

Biosensor for E. coli O157:H7 DNA detection

Low detection limit for DNA (a few hundreds of pmol), rapid label-free and easy-to-use bacteria detection, which holds the potential for future use in various ss-DNA analyses by integrated into a self-contained biochip.

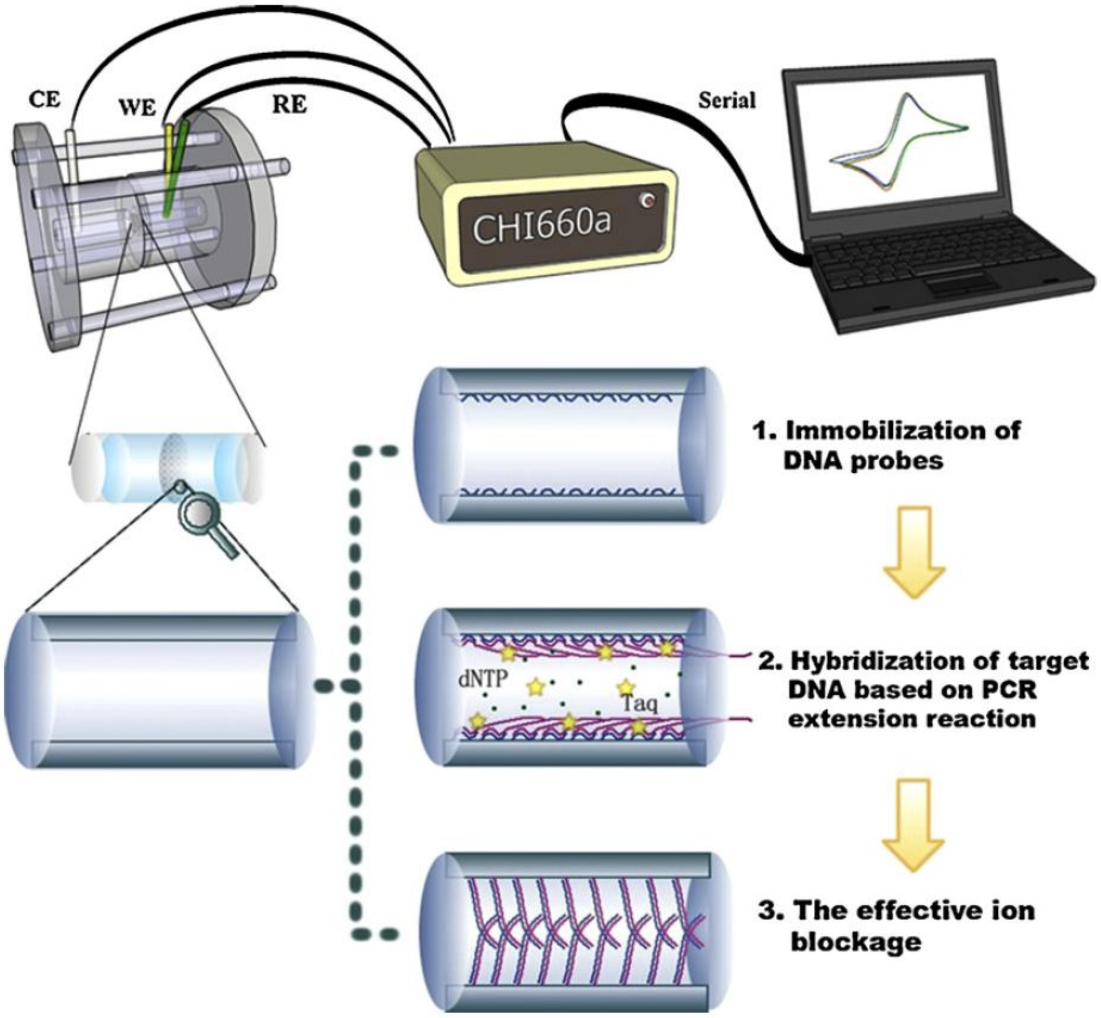

Formation of a porous alumina electrode as a low-cost CMOS neuronal interface

Controlled and low-cost method of fabricating

CMOS multiple electrode arrays with good corrosion resistance and a nanoporous morphology conducive to good cell adhesion.

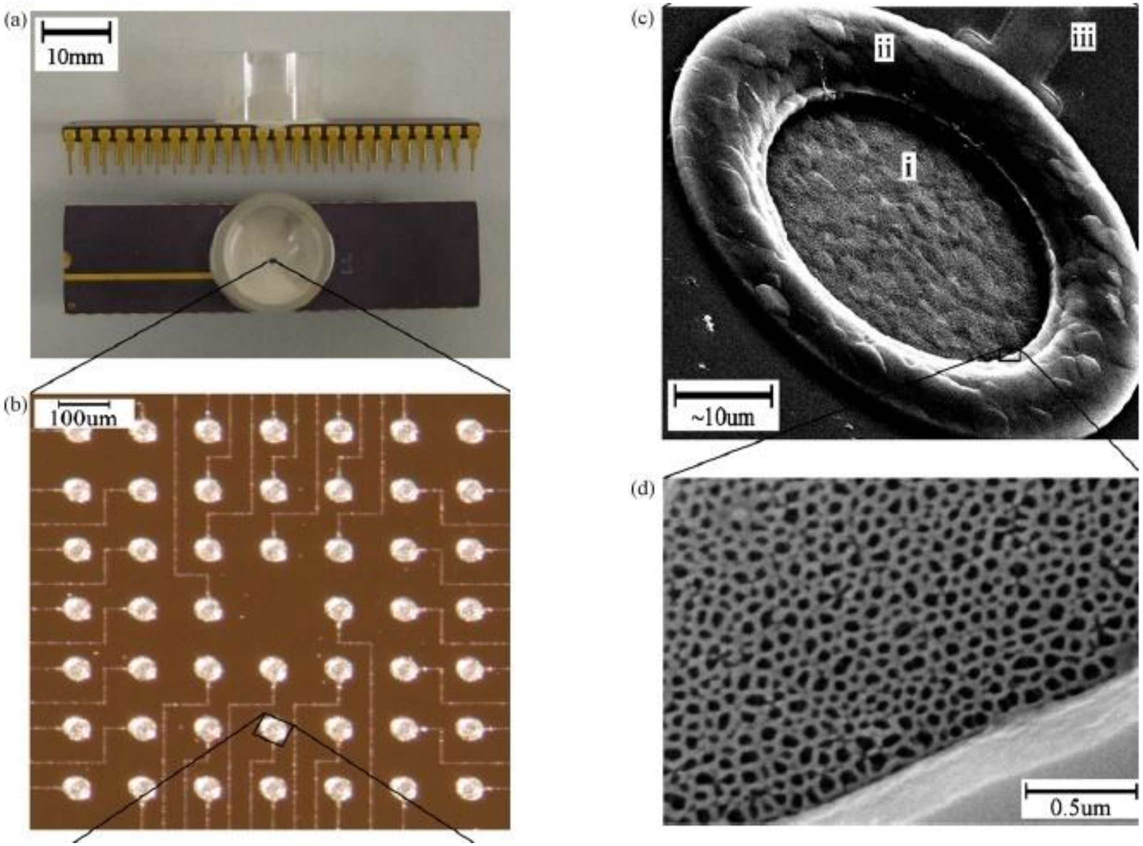

Platinum nanowire nanoelectrode array for the fabrication of biosensors

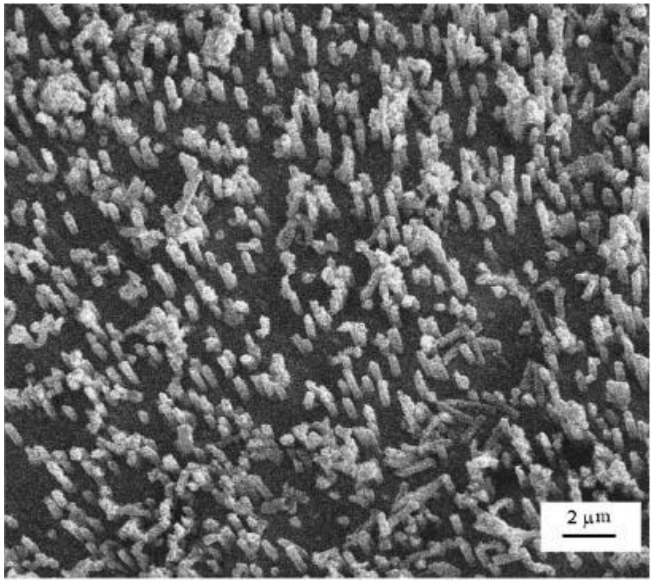

SEM image of the platinum nanowire array

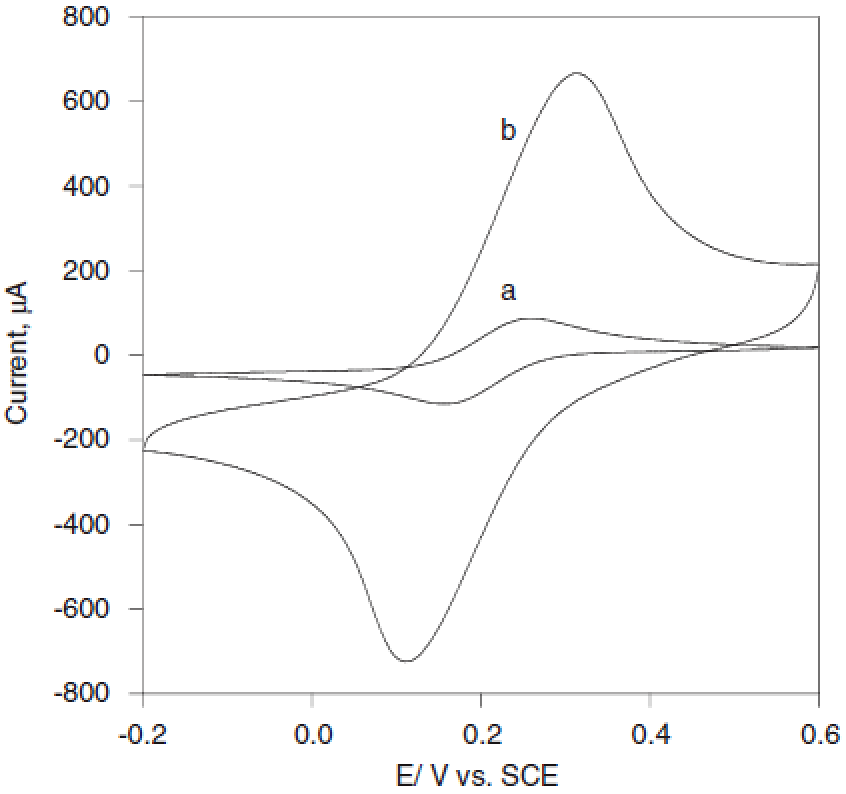

Cyclic voltammograms of (a) conventional platinum and (b) platinum NEA in 20 mM $K_3Fe(CN)_6$ containing 0.2 M KCl. Scan rate 100 mV s^{-1}.

Optical waveguides

Porous anodic alumina waveguide for high sensitivity (bio-) chemical sensing with bovine serum albumin adsorption and desorption at various pH values, with subangstrom sensitivity in the effective thickness of protein adsorbed.

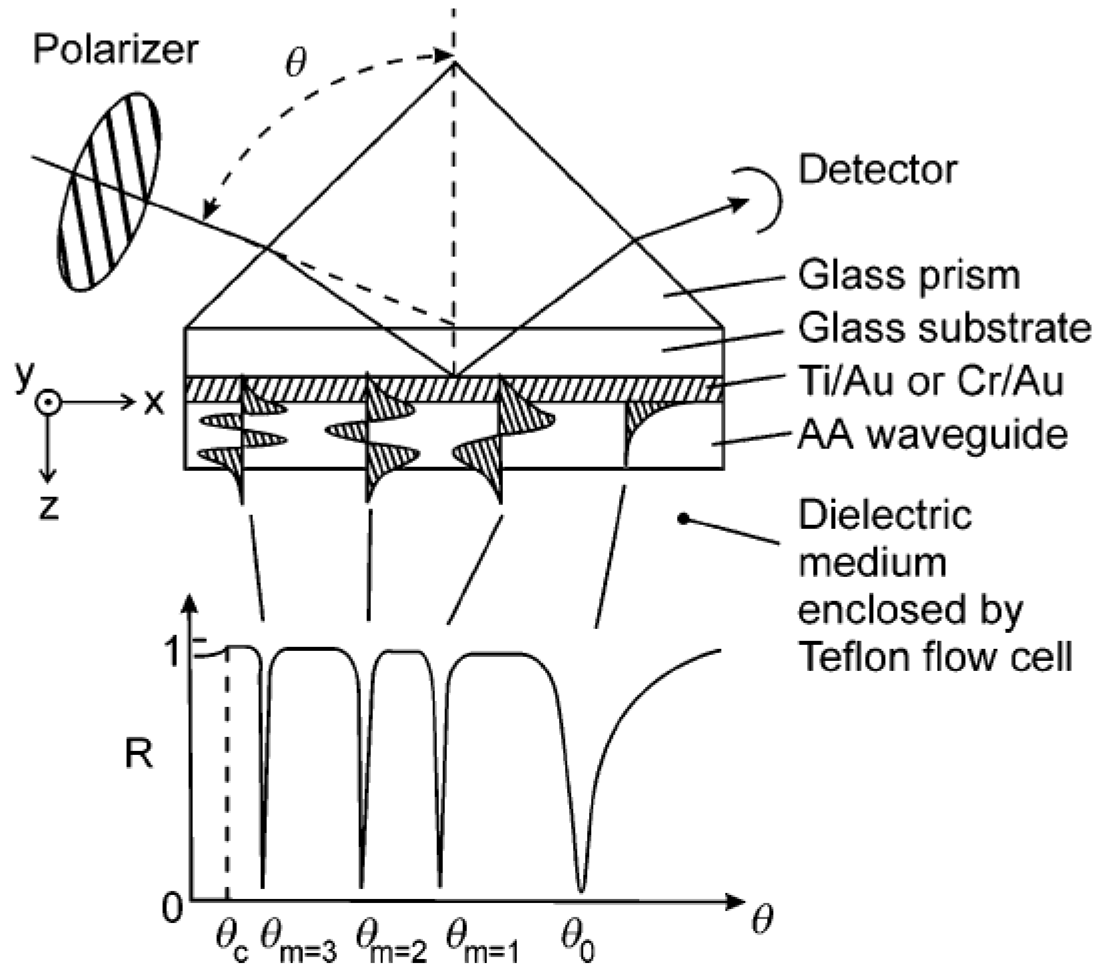

Catalytic membrane reactors

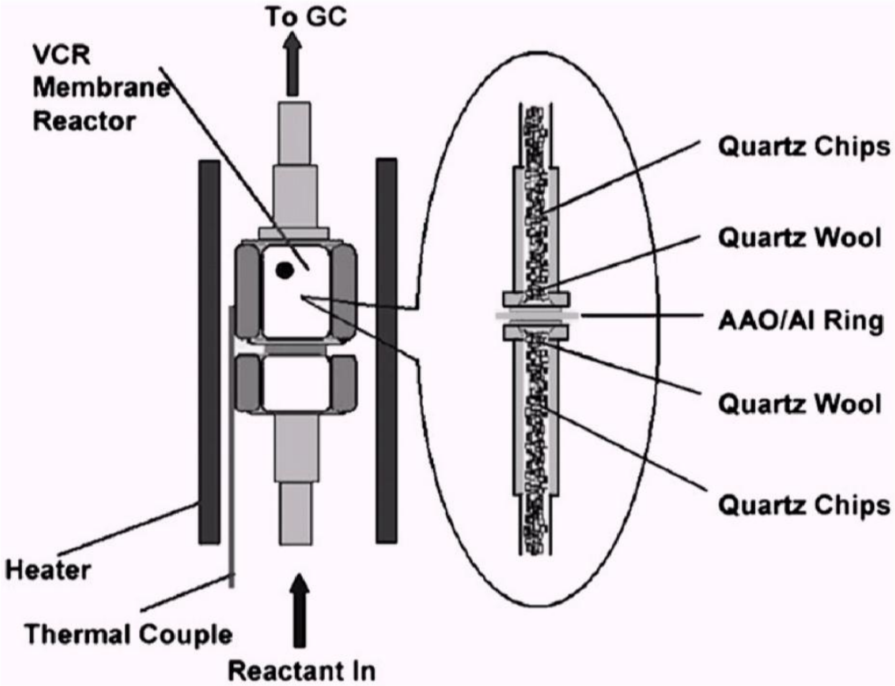

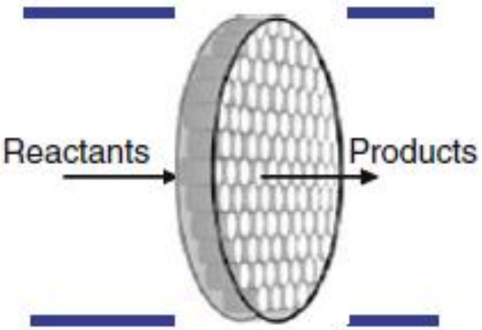

For the oxidative dehydrogenation (ODH) of cyclohexane, the nanolith catalytic system is superior to a conventional powdered catalyst in terms of both efficiency and in reducing over oxidation

H. Feng et al. / Chemical Engineering Science 64 (2009) 560 – 567; P.C. Stair et al. / Topics in Catalysis Vol. 39, Nos. 3–4, October 2006 nanomaterials.it

Synthesis of nanoscale polymer spheres, capsules or rods

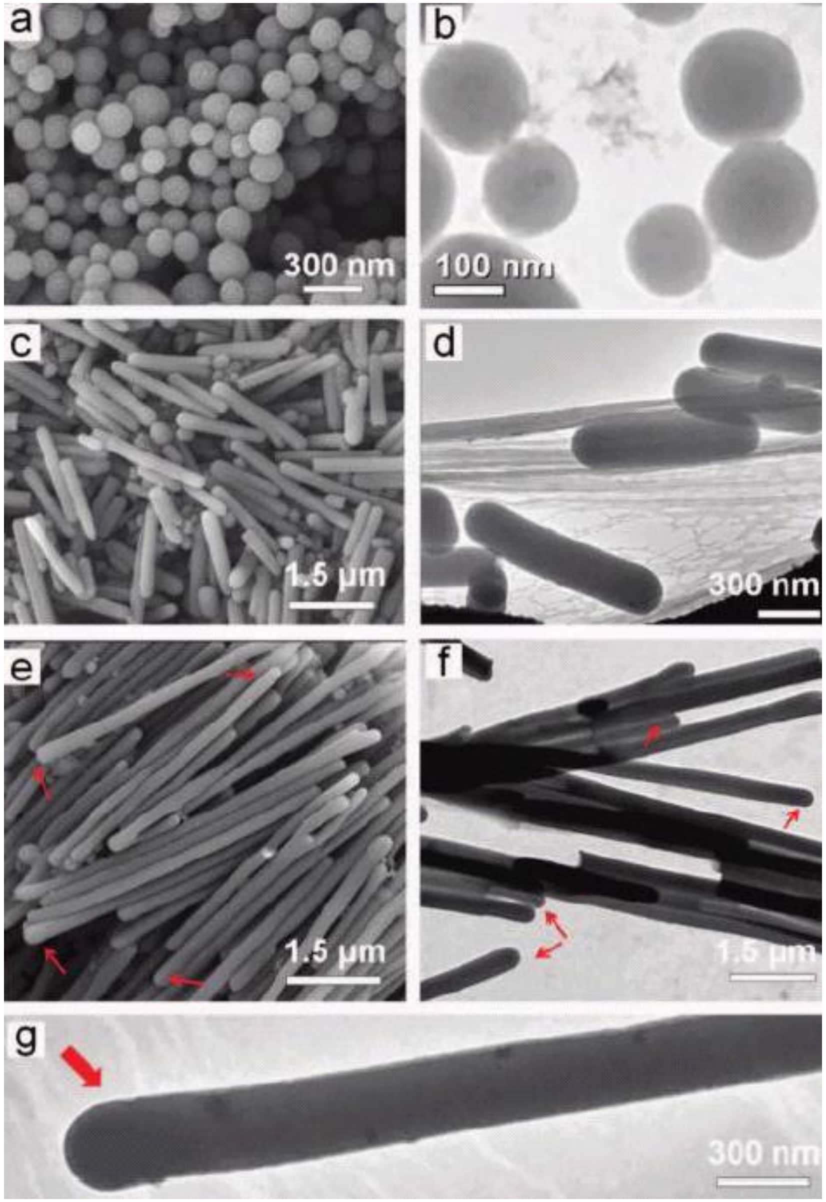

Polystyrene nanostructures resulting from polystyrene / tetrahydrofuran solutions. a and b) for 20 mg/mL; (c and d) for 40 mg/mL; (e-g) for 150 mg/mL.

X. Feng and Z. Jin / Macromolecules, Vol. 42, No. 3, 2009, 569-572

Fabrication of ordered Ni nanocones using a porous anodic alumina template

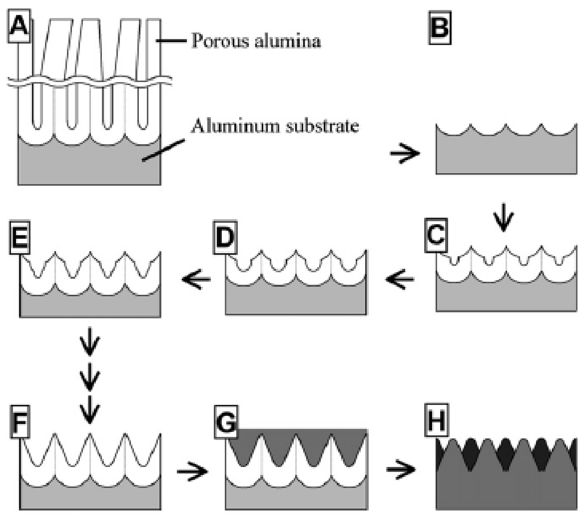

Fabrication procedure of Ni nanocones and nano-conical film. Long-period anodization (A), ordered concaves (B), first anodization (C), pore widening (D), second anodization (E), conical template (F), Ni nanocones (G), Ni nano-conical film (H).

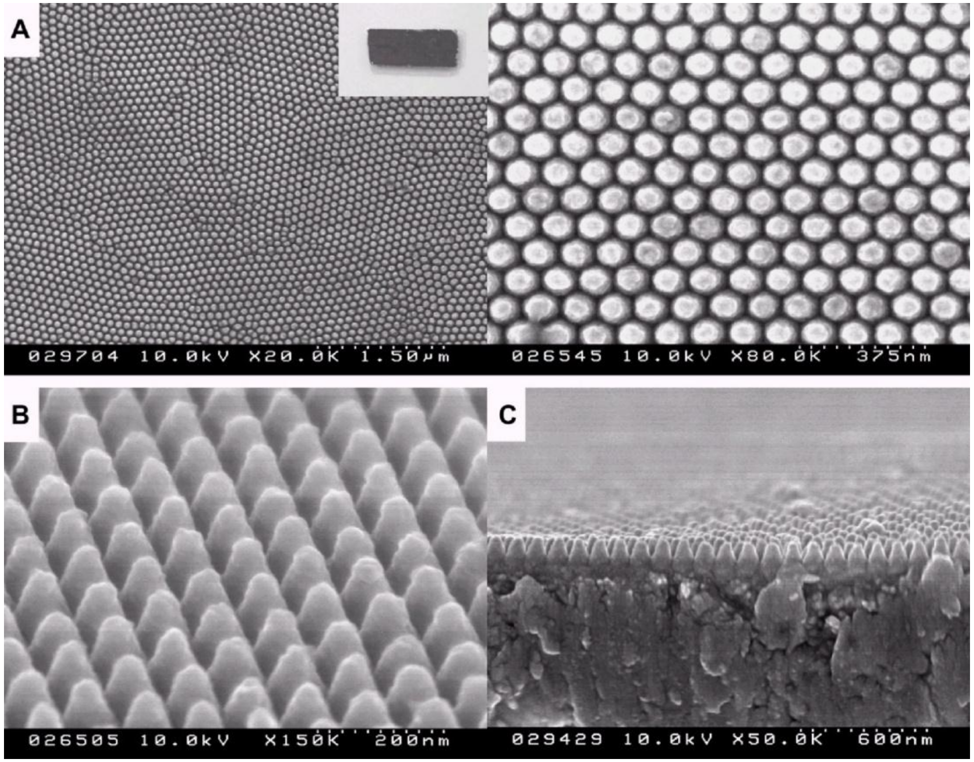

Fabrication of a tungsten master stamp using self-ordered porous alumina

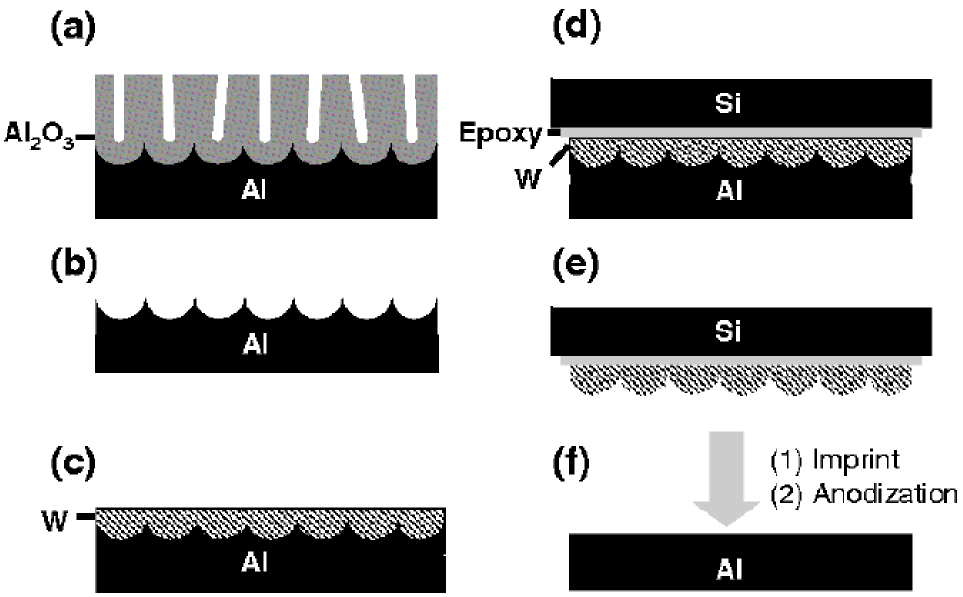

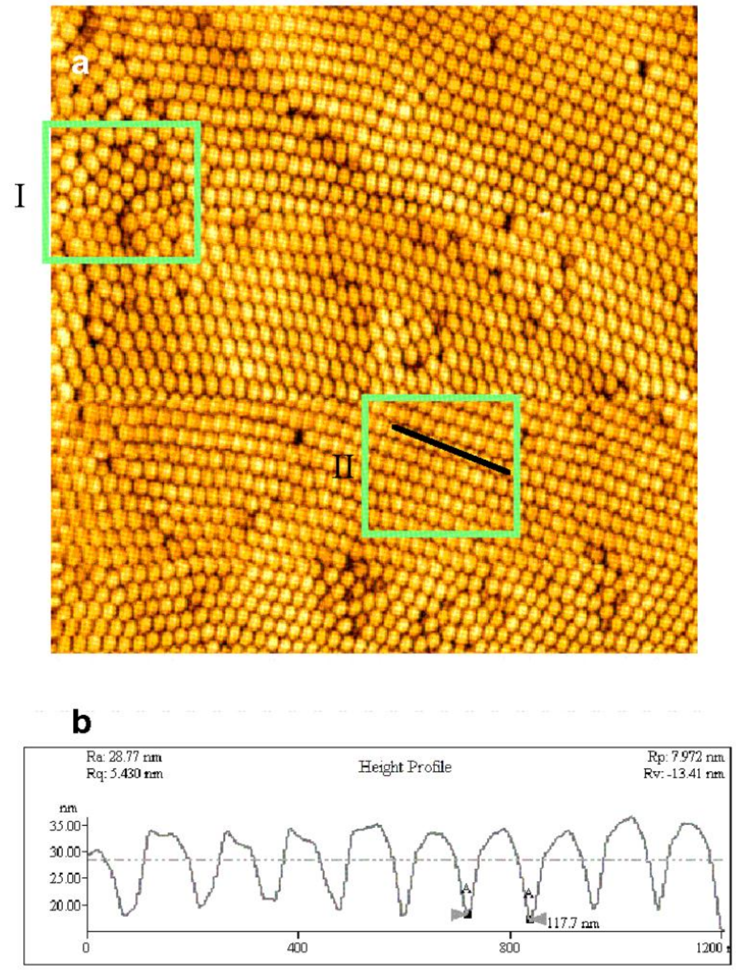

Nanotubular TiO_2 microvalve actuated by UV light

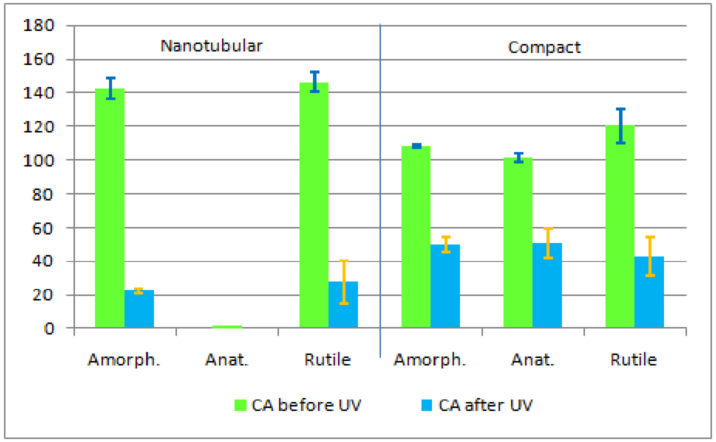

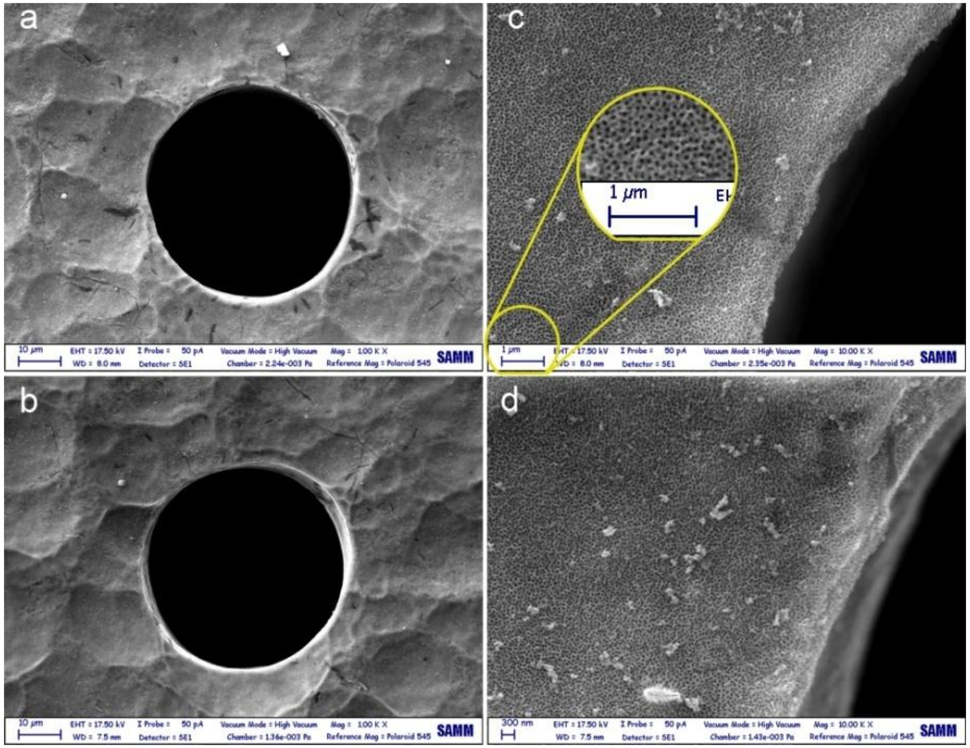

Contact angle measurement of different TiO_2 layers before and after UV irradiation.

Low-voltage electro-osmotic pumping using porous anodic alumina membranes

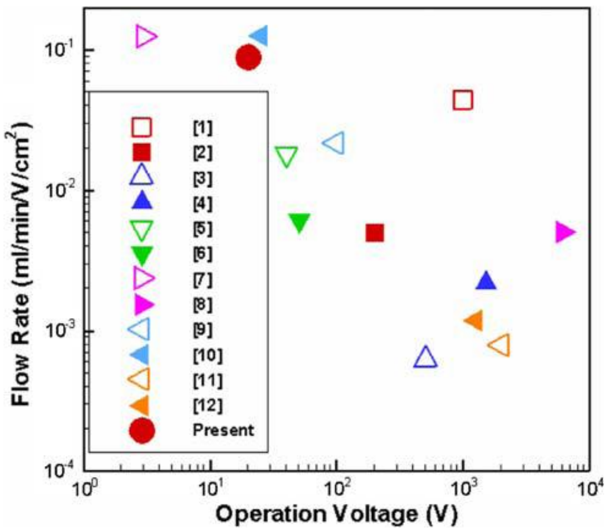

Comparison of the flow rate between this study and other literature values

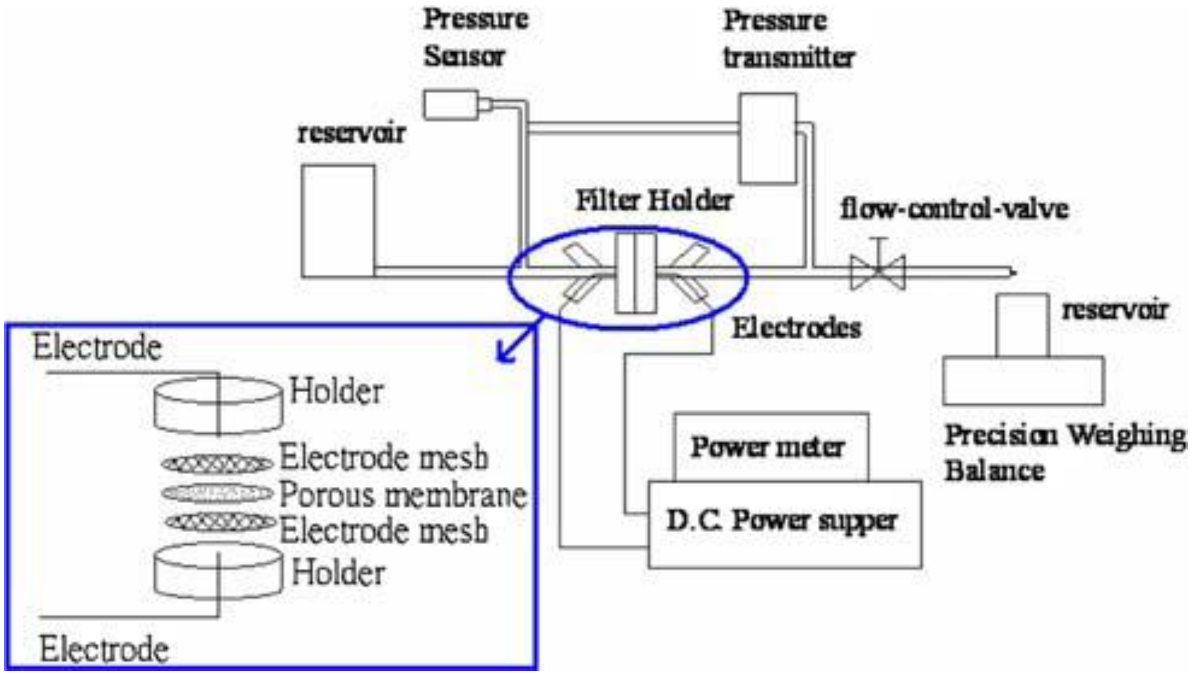

Fabrication of Arrays of Metal and Metal Oxide Nanotubes by Shadow Evaporation

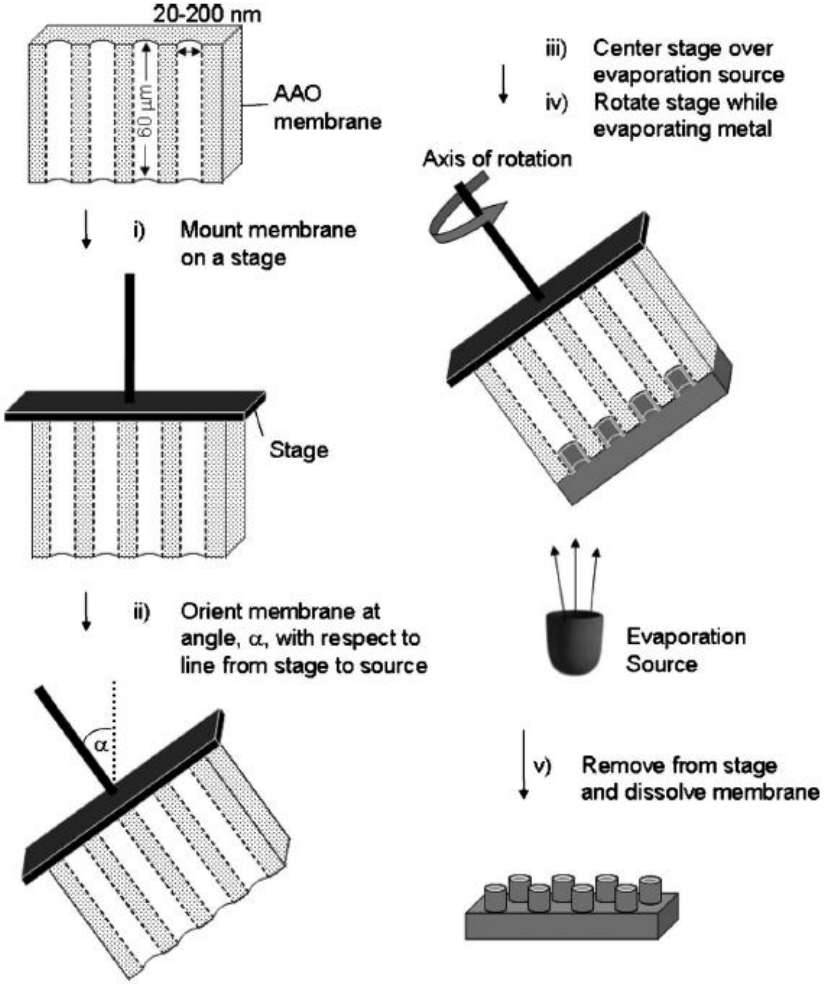

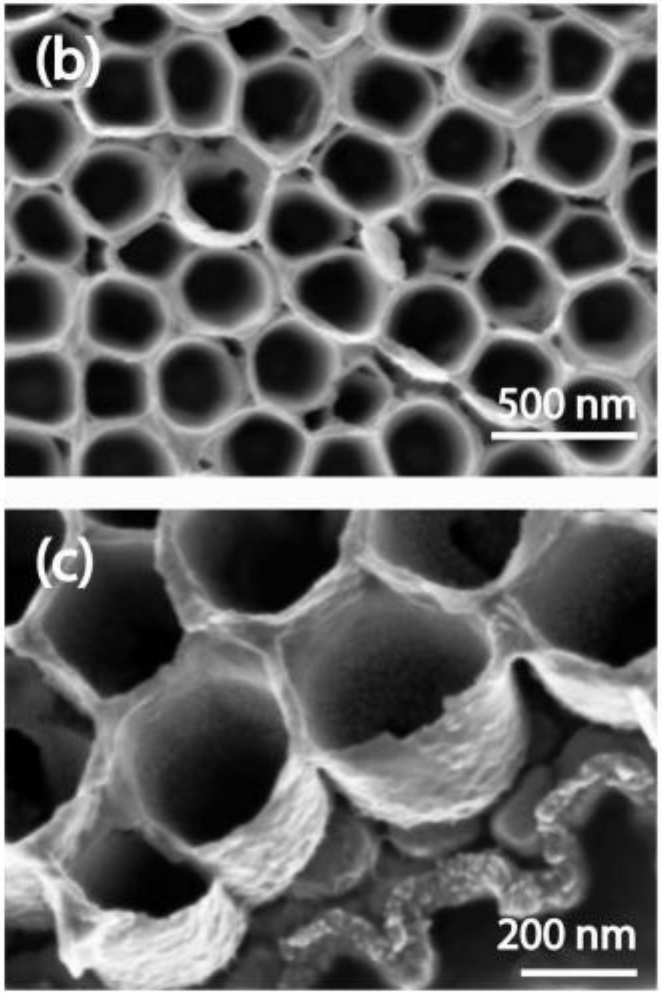

M. D. Dickey et el. / ACS Nano VOL. 2 ・NO. 4 ・800–808 ・2008

SERS enhancement by means of silver-nanowire array fabricated by AAO template

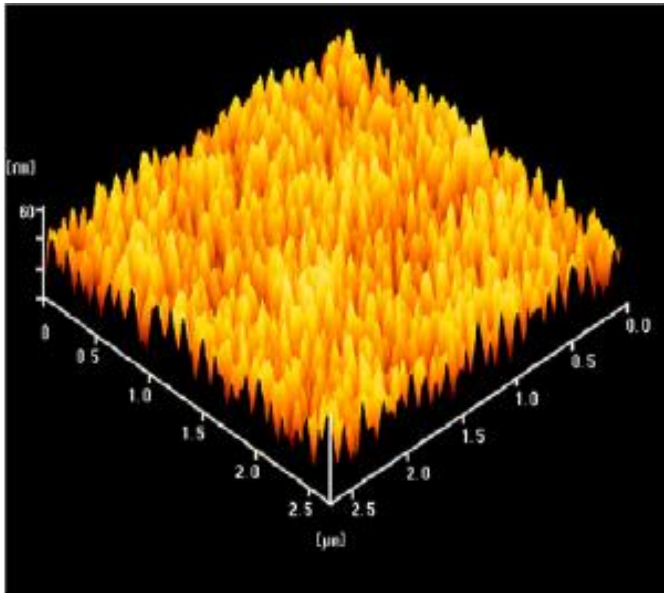

AFM micrograph of Ag nanowires after the partial alumina layers is dissolved.

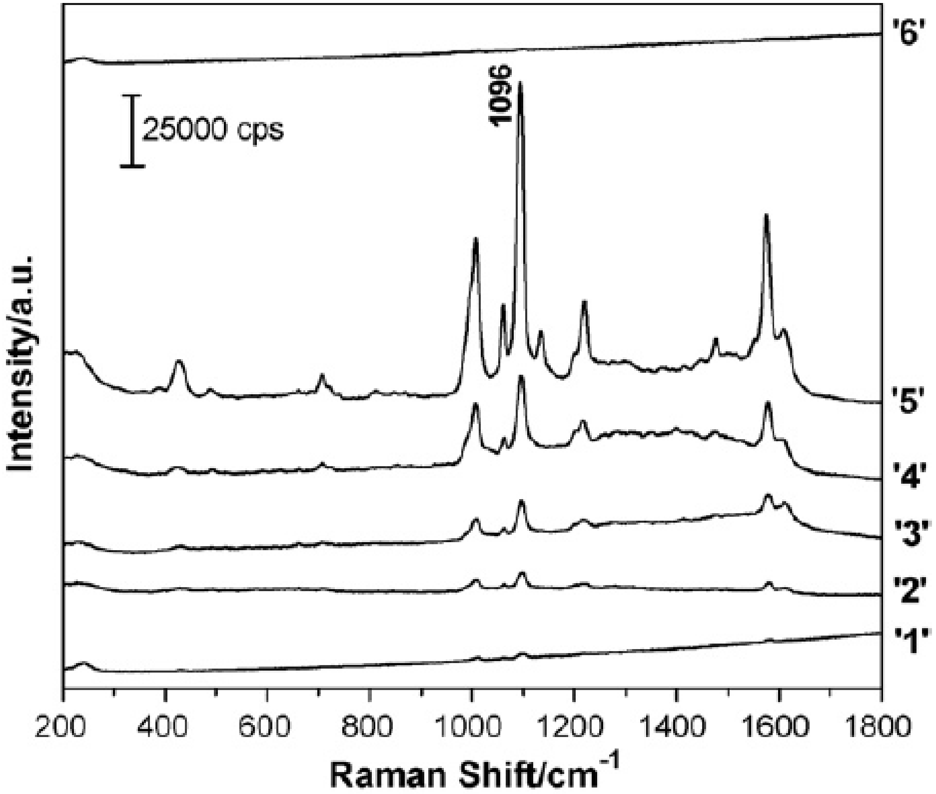

SERS spectra of 4-MPy adsorbed on Ag nanowires with same diameter, but different heights. ‘1’: 0 nm, ‘2’: 50 nm, ‘3’: 108 nm, ‘4’: 215 nm, ‘5’: 270 nm, and ‘6’: collapsed.

Magnetic Co–Pt nanowire arrays in AAO templates

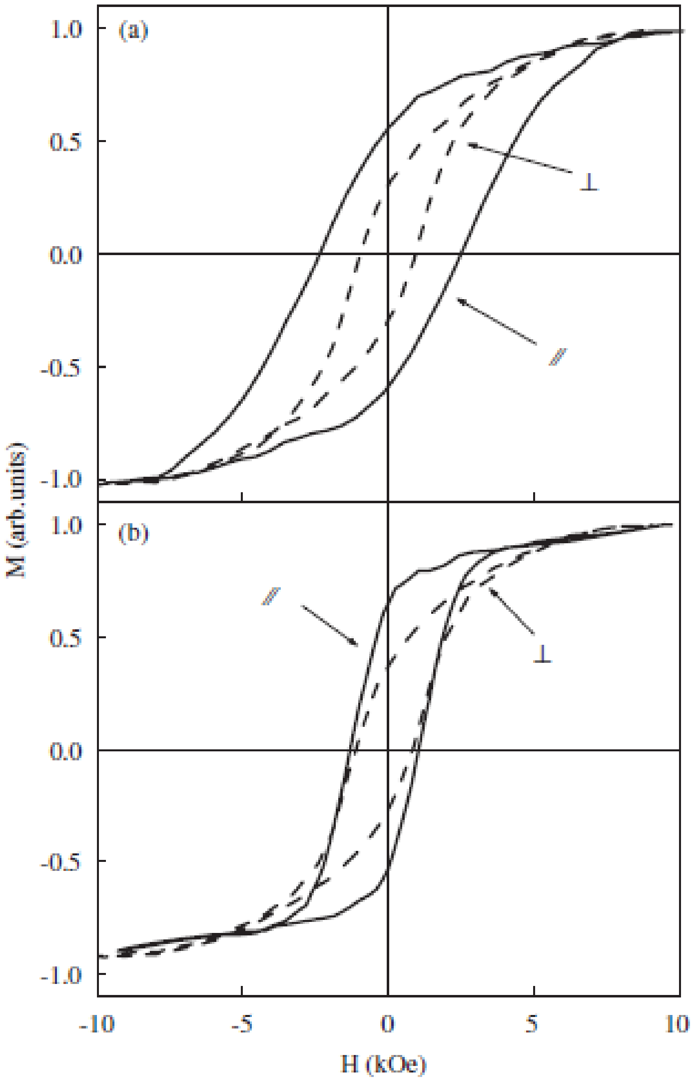

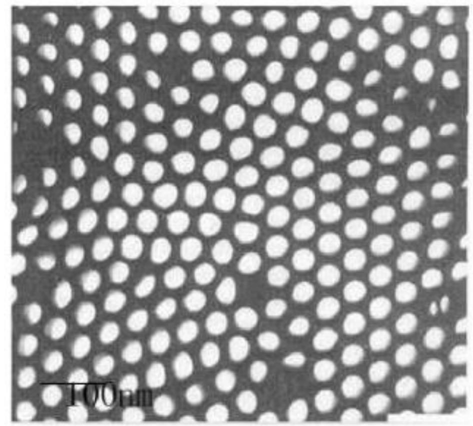

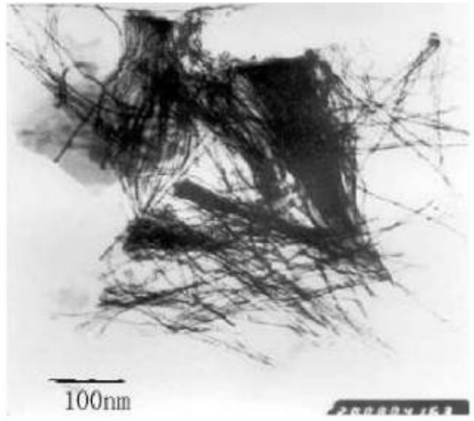

(a) Plan-view TEM micrograph of an AAO template with 40nm diameter holes. (b) TEM image of Co–Pt nanowires liberated from AAO template.

Magnetization hysteresis loops for an array of (a) 40nm and (b) 80nm diameter Co–Pt nanowires in AAO templates. The solid and dash curves refer to the parallel and perpendicular geometries, respectively.

Porous anodic alumina microreactors for production of hydrogen from ammonia

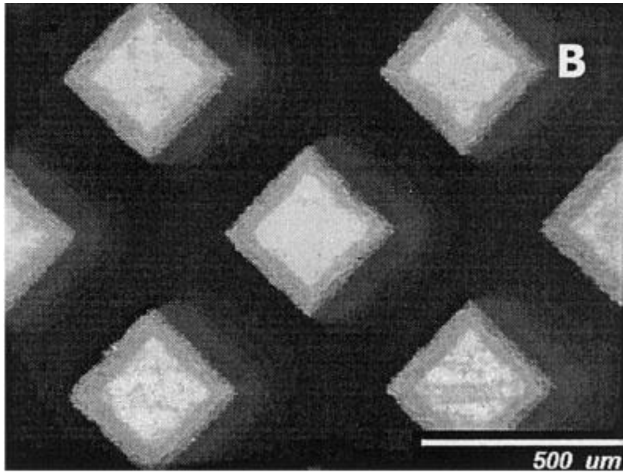

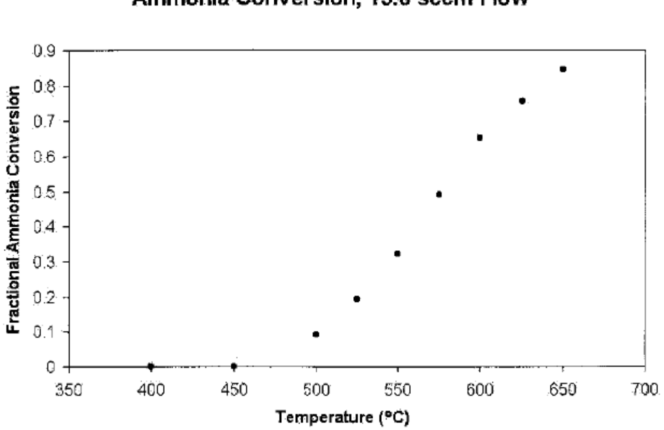

Arrays of monolithic anodized aluminum posts are useful catalyst supports for microreactors. The posted structures stay in place in the microreactor, and they do not suffer from the fluid bypassing that plagues other previous microreactor designs. The surface areas are modest compared to supported catalysts, but large compared to the bare metal and washcoated monolithic microreactor designs. The structures have shown the ability to withstand significant thermocycling, and show substantial catalytic activity when impregnated with metal

Coupled semiconductor by filling 1D TiO_2 nanotubes with CdS

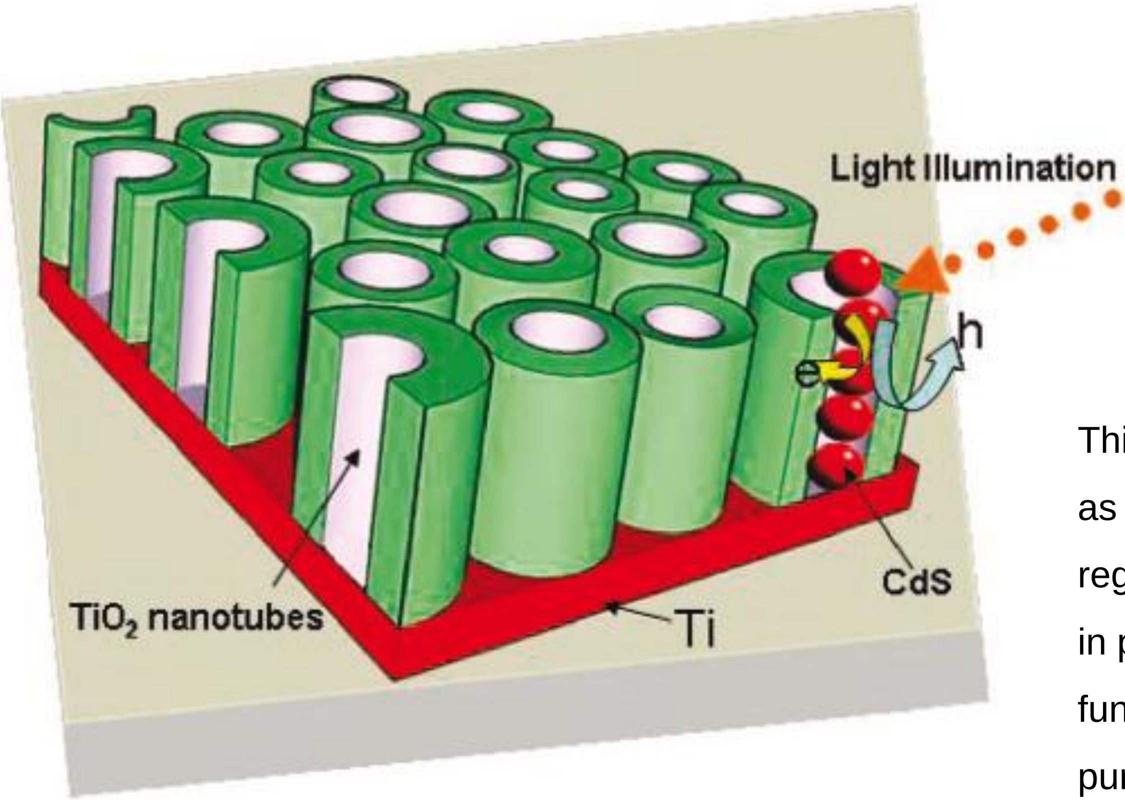

This material harvests solar light in UV as well as visible light (up to 510 nm) region. An eight to 9-fold enhancement in photoactivity is observed using CdS functionalized TiO2 NTs compared to pure TiO2 NTs and commercial P25 NPs.

S. Banerjee **et al. /** *Chem. Mater.* ***2008, 20, 6784–6791***

Nanoporous anodic alumina capsules

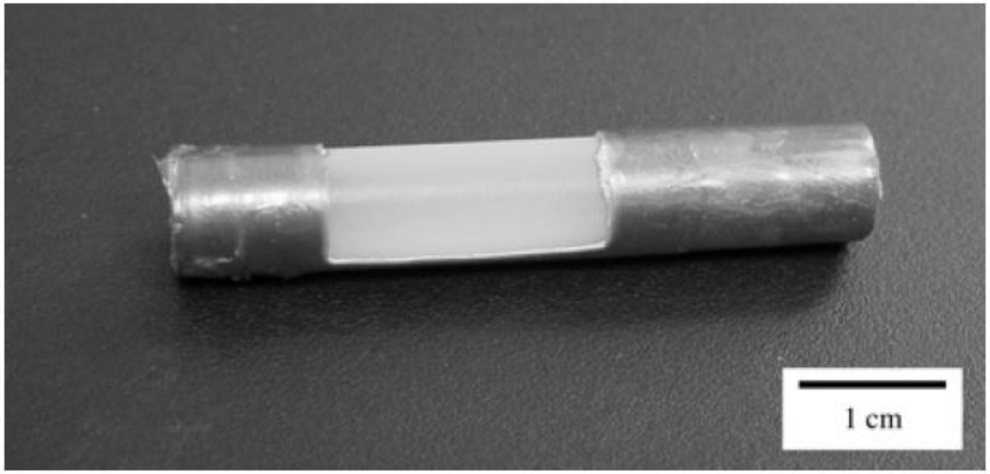

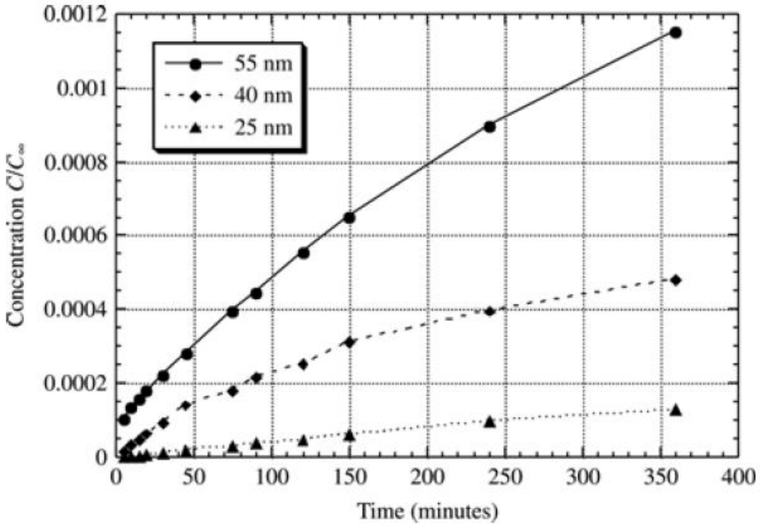

Release fluorescein (400 Da) from AAO capsules of 25 nm, 45nm and 55 nm pore diameters.

D. Gong et al. / Biomedical Microdevices 5:1, 75-80, 2003.

Percolation threshold of silver and copper nanowires in polystyrene composites

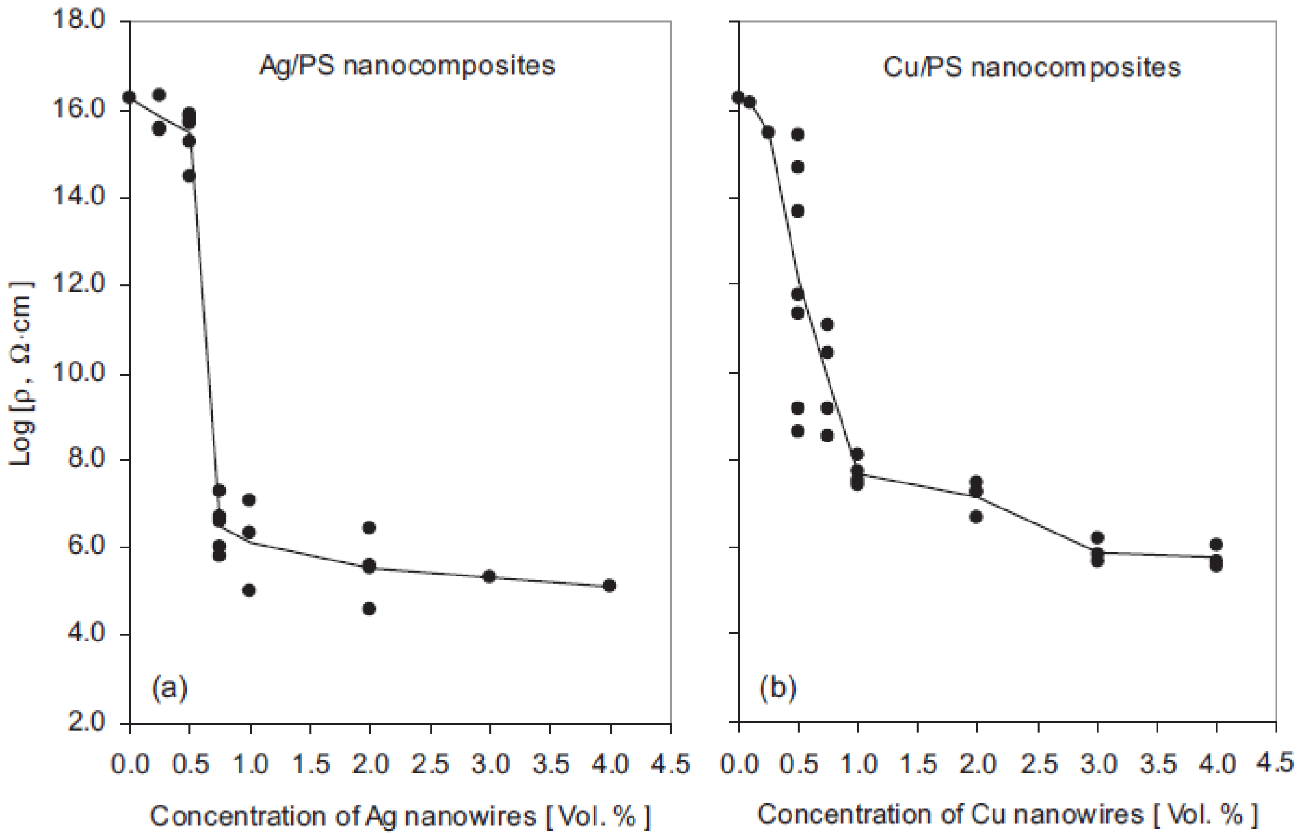

Volume electrical resistivity (q) of PS nanocomposites for different concentrations of a) Ag and b) Cu nanowires

Surface coatings for improvement of bone cell materials and antimicrobial activities of Ti implants

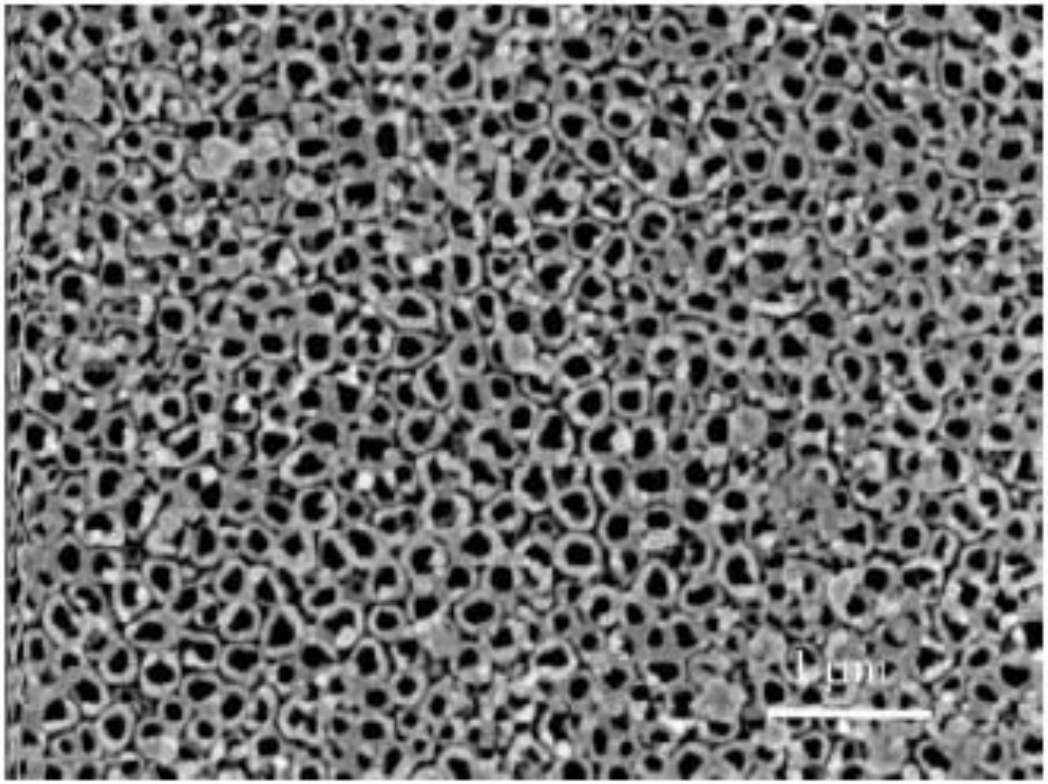

Ti surface was modified by growing in situ titania nanotube via anodization process. Nanotube surface with and without silver electrodeposition showed good cell-to-cell attachment, high cell proliferation and enhanced bone cell–material interactions in comparison to Ti-control. The Ag deposited nanotube surface had an antibacterial activity over 99% against the growth of colonies of Pseudomonas aeruginosa where as Ti control and nanotube surfaces had no influence on the growth of colonies of Pseudomonas aeruginosa

Das et al / Journal of Biomedical Materials Research Part B: Applied Biomaterials 2008

TiO_2 nanotube for the photocatalytic splitting of water

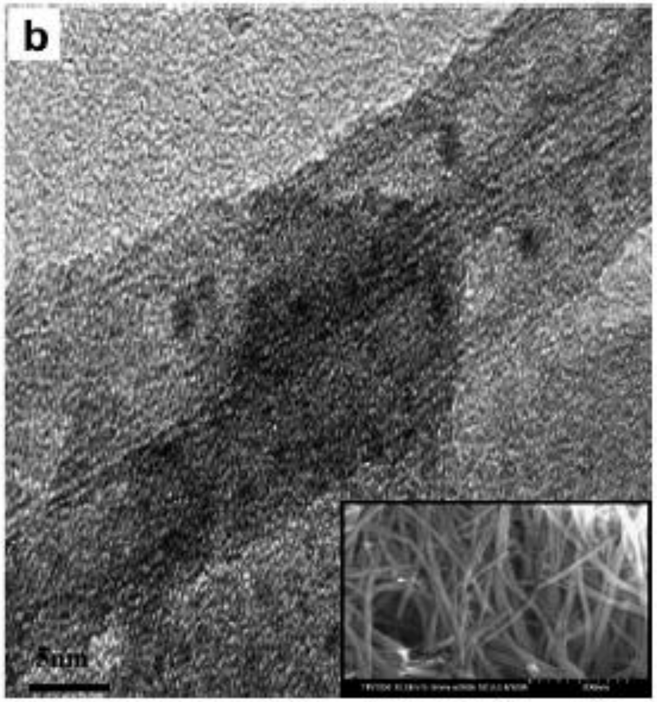

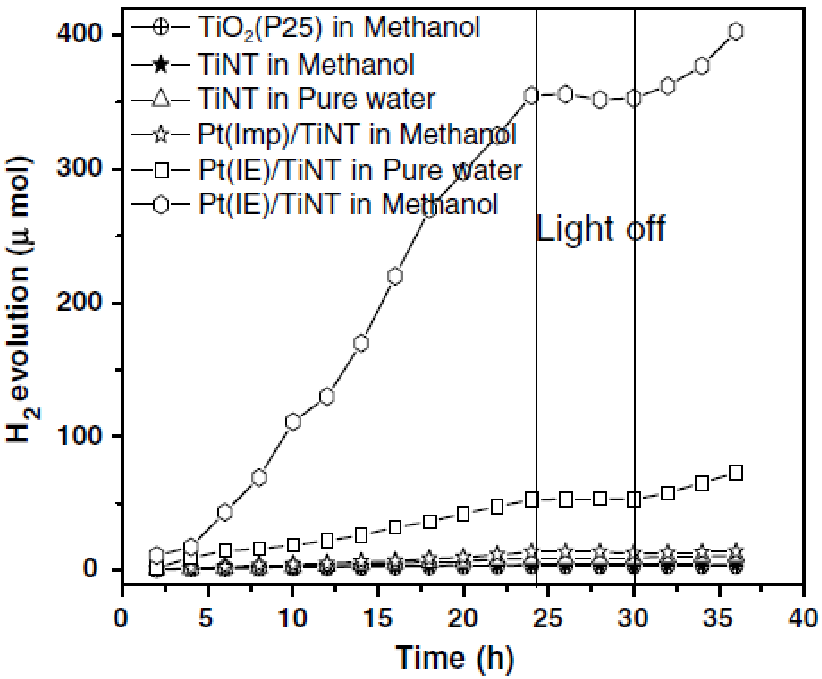

the Pt ion-exchanged titania nanotube, Pt(IE)/TiNT, was highly active for the stoichiometric production of hydrogen, 14.6 (in methanol solution) and 2.3 (in pure water) μmol H_2/h from the splitting of water under visible light.

Enhancement of the light extraction efficiency in organic light emitting diodes utilizing a AAO film

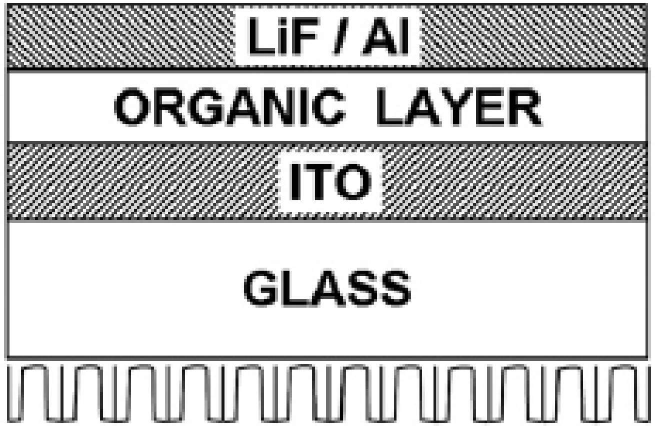

OLEDs with the porous alumina film deposited on the bottom of device.

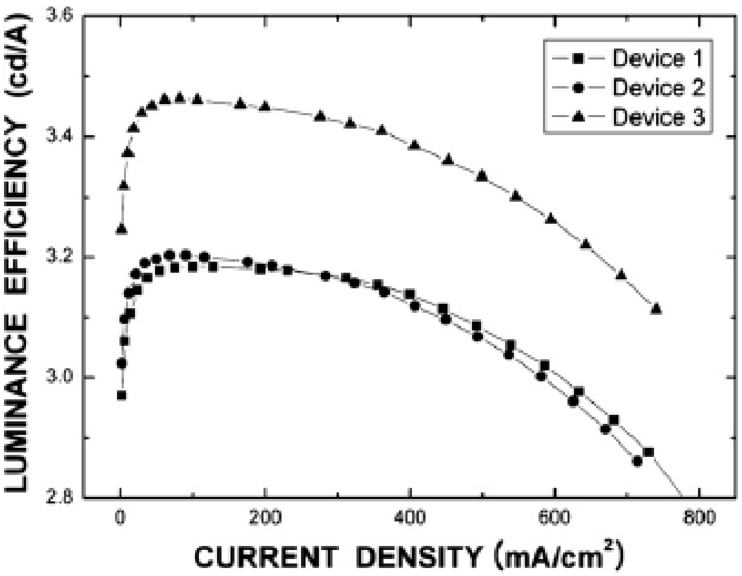

Luminance efficiencies as functions of the current density for OLEDs with various structures

Synthesis of polydiphenylamine nanofibrils through AAO template

Polymerization of PDPA fibrils inside the pores of AAO template carried out in potential dynamic mode by cycling the potential from −0.2 to 1.4V versus SCE . The electrolyte consisted of 1.0 mol L^{-1} $HClO_4$ containing 0.01 mol L^{-1} of diphenylamine.

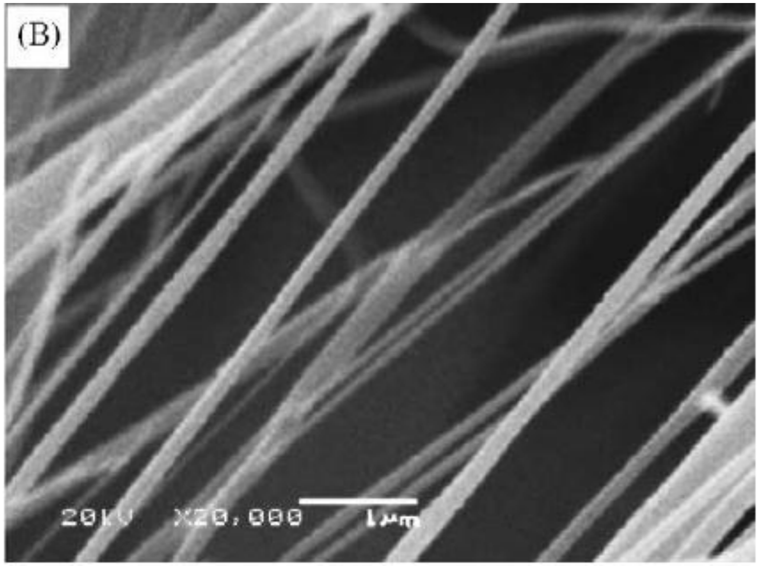

The spatial restraint in the pores of AAO membrane induces the formation of more ordered PDPA chains in the AAO membrane.

DNA-templated silver nanowires for ammonia gas sensor

DNA-templated silver nanowires have been deposited on gold electrode for ammonia gas sensors at room temperature.

The material possesses high selectivity, quick gas response and fast recovery at room temperature.

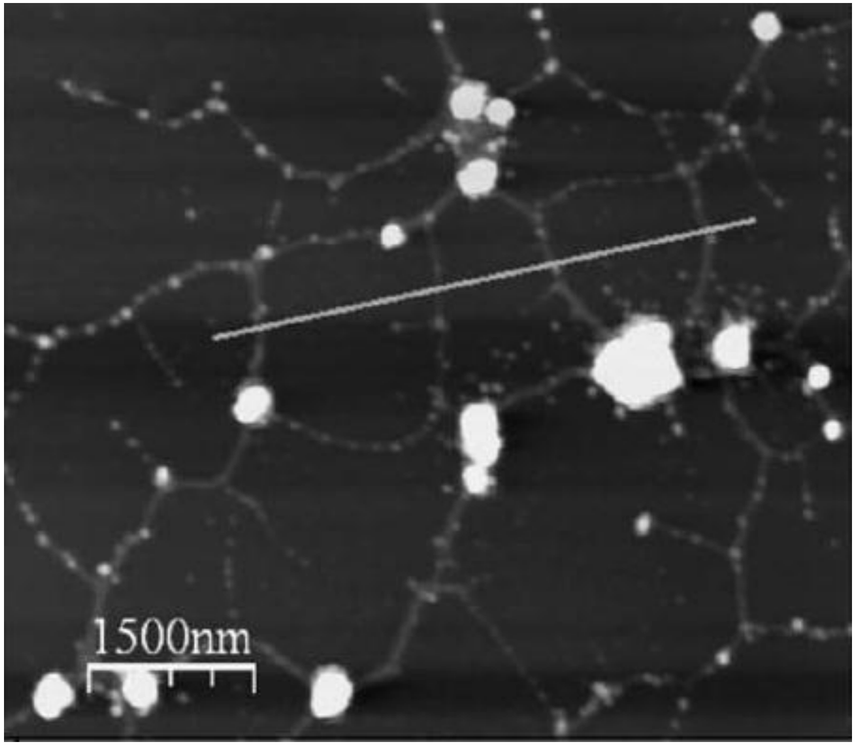

Superhydrophobic polyurethane film molded on a porous anodic alumina template

The water contact angle on a molded PU film surface is approximately 152° , while it is 85° on a free surface formed in air.

Super-hydrophobicity is a result of the enhanced roughness, which is modulated by a well-designed PAA template surface morphology.

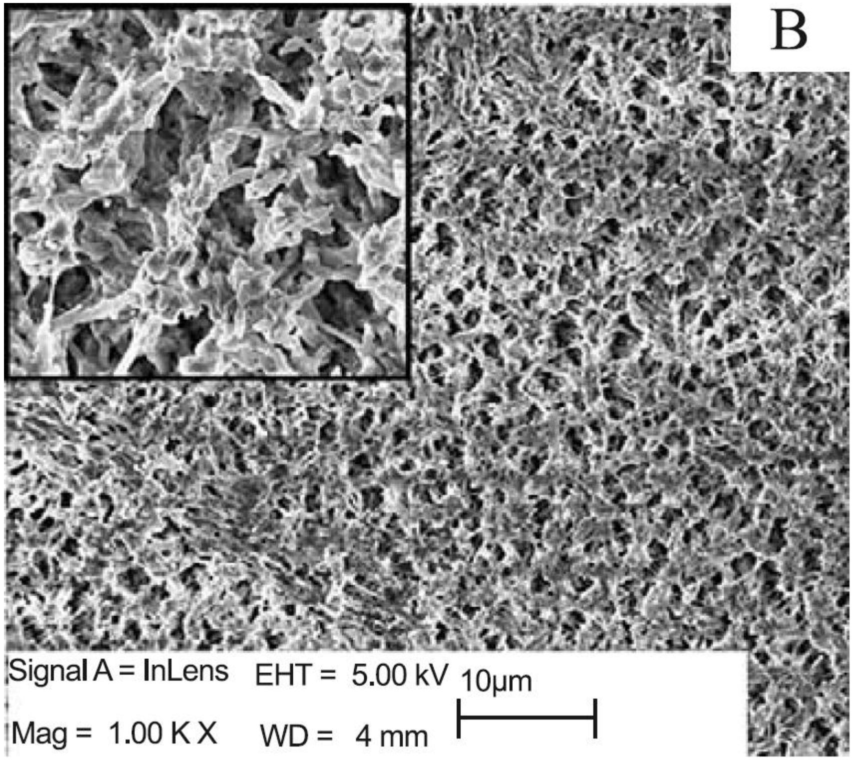

TiO_2 nanotube membrane for flow-through photocatalytic applications

Preparation of a freestanding TiO_2 membrane by a three-step process:

(i) Growth of a high aspect ratio TiO_2 nanotubular layer on Ti.

(ii) Selective dissolution of the metallic substrate,

(iii) Opening of the closed tube bottom by selective chemical etching

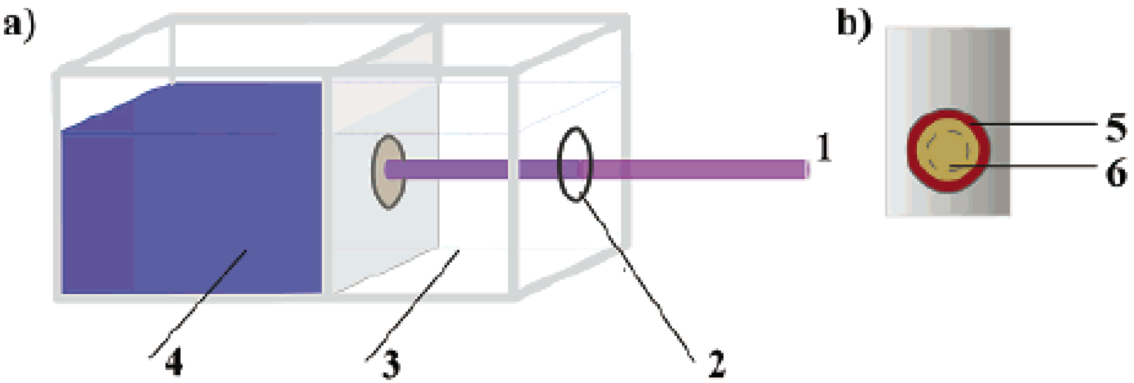

Figure 2. Schematical representation of the setup used for flow-through photocatalytic experiments. The chamber on the right is filled with distilled water, the chamber on the left is filled with MB, and between them a TiO_2 membrane is glued on a holder with an opening (1, laser; 2, quartz window; 3, distilled water; 4, MB; 5, epoxy glue; 6, TiO_2 nanotubular membrane).

Capacitive humidity sensor based on anodic aluminum oxide

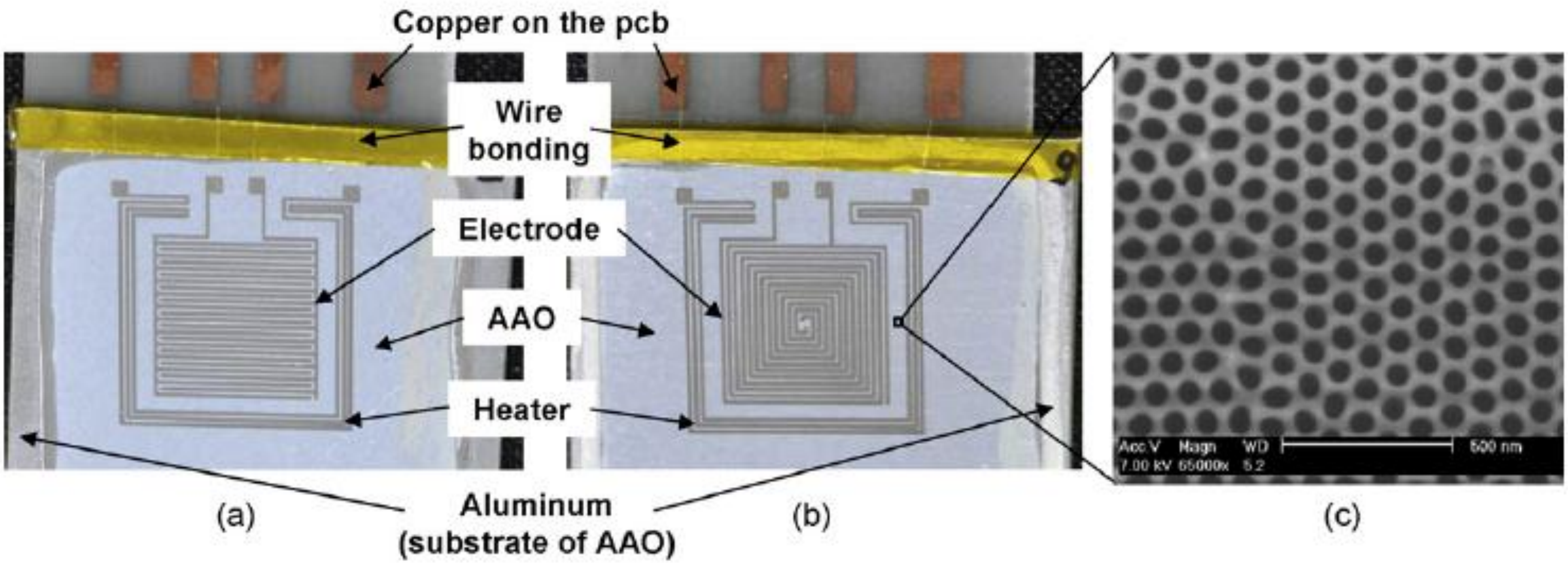

Humidity sensor devices: (a) interdigitated type (b) rectangular spiral-shaped type

Humidity sensor structures with thin film porous alumina for on-chip integration

The constructed AAO-based sensors – using both the annealed palladium and electroplated gold-grid as upper electrode – were highly sensitive to ambient RH changes, the highest average sensitivity was approx. 15 pF/RH%.

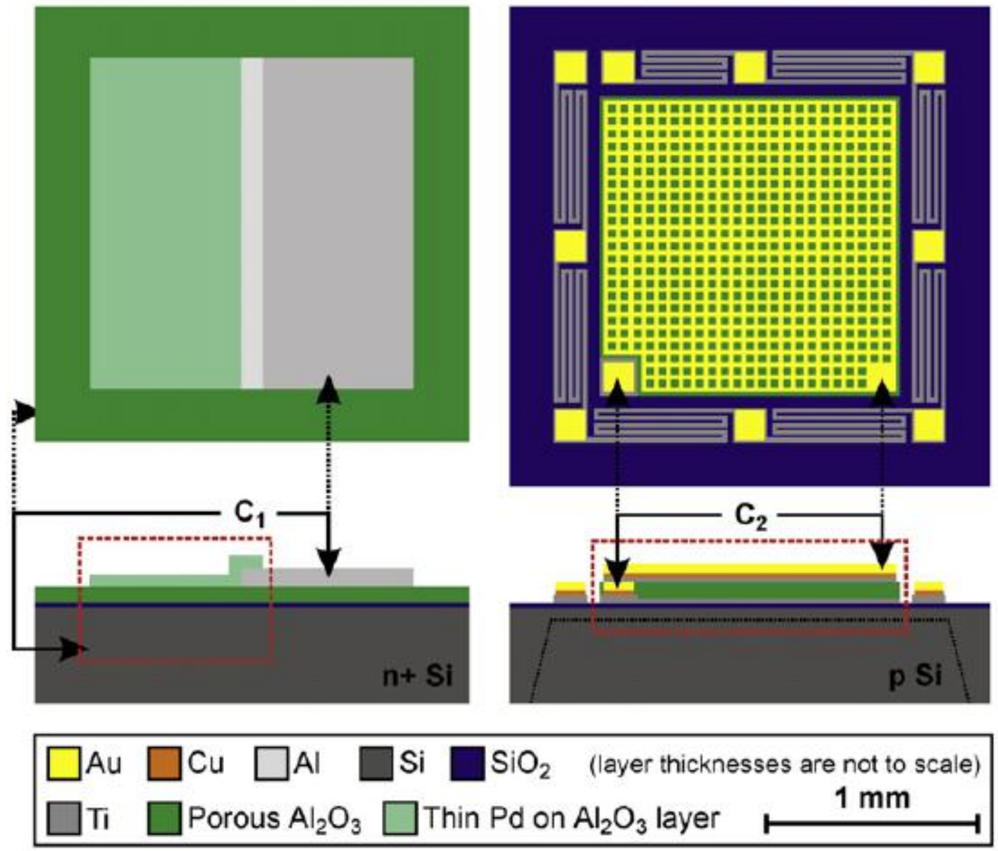

L. Juhász, J. Mizsei / Thin Solid Films 517 (2009) 6198–6201

Porous anodic alumina for chromatography chip system

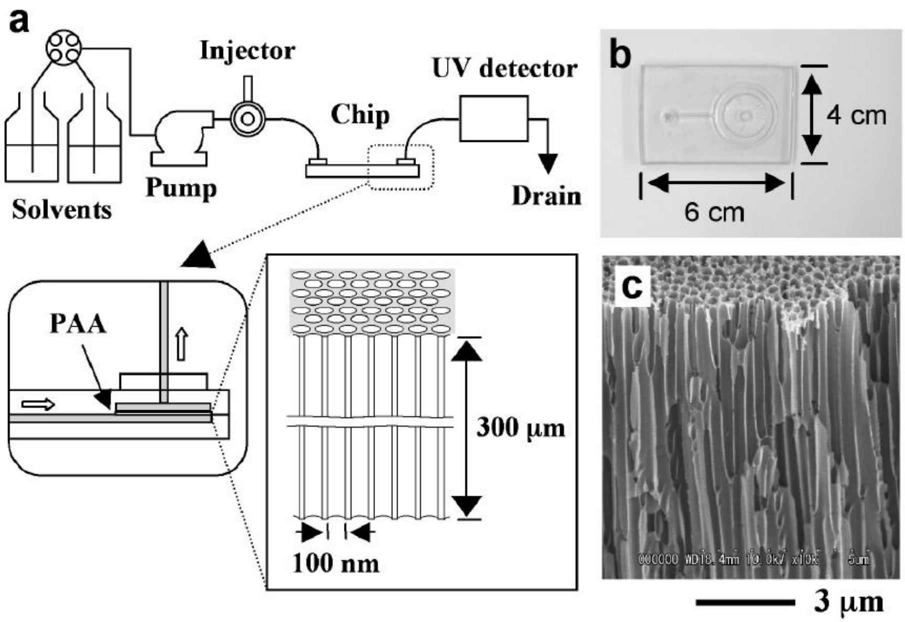

Experimental setup for chromatographic measurement. (a) Schematic illustration of chromatographic system. (b) Picture of chromatography chip. (c) Cross-sectional SEM image of PAA membrane

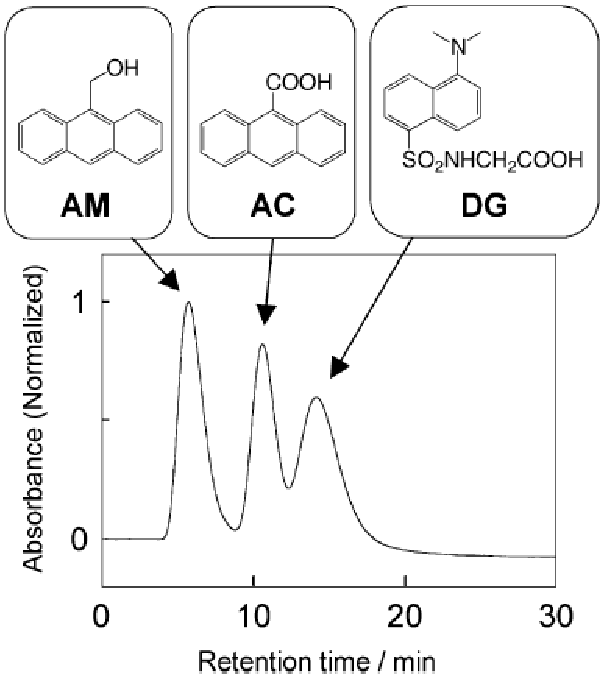

Chromatogram of mixture of AM, AC, and DG by chromatography chip